OPEN ACCESS Freely available online

PLOS ONE

Mathematical Modeling of Interleukin-35 Promoting Tumor Growth and Angiogenesis

Kang-Ling Liao[1]*, Xue-Feng Bai[2], Avner Friedman[1,3]

1 Mathematical Biosciences Institute, The Ohio State University, Columbus, Ohio, United States of America, **2** Department of Pathology and Comprehensive Cancer Center, The Ohio State University, Columbus, Ohio, United States of America, **3** Department of Mathematics, The Ohio State University, Columbus, Ohio, United States of America

Abstract

Interleukin-35 (IL-35), a cytokine from the Interleukin-12 cytokine family, has been considered as an anti-inflammatory cytokine which promotes tumor progression and tumor immune evasion. It has also been demonstrated that IL-35 is secreted by regulatory T cells. Recent mouse experiments have shown that IL-35 produced by cancer cells promotes tumor growth via enhancing myeloid cell accumulation and angiogenesis, and reducing the infiltration of activated $CD8^+$ T cells into tumor microenvironment. In the present paper we develop a mathematical model based on these experimental results. We include in the model an anti-IL-35 drug as treatment. The extended model (with drug) is used to design protocols of anti-IL-35 injections for treatment of cancer. We find that with a fixed total amount of drug, continuous injection has better efficacy than intermittent injections in reducing the tumor load while the treatment is ongoing. We also find that the percentage of tumor reduction under anti-IL-35 treatment improves when the production of IL-35 by cancer is increased.

Citation: Liao K-L, Bai X-F, Friedman A (2014) Mathematical Modeling of Interleukin-35 Promoting Tumor Growth and Angiogenesis. PLoS ONE 9(10): e110126. doi:10.1371/journal.pone.0110126

Editor: Raffaele A Calogero, University of Torino, Italy

Received April 8, 2014; **Accepted** September 17, 2014; **Published** October 30, 2014

Data Availability: The authors confirm that all data underlying the findings are fully available without restriction. All relevant data are within the paper.

Funding: This work is supported, in part, by the National Science Council of Taiwan, R. O. C. (http://web1.nsc.gov.tw/) under No. NSC 101-2917-I-564-062, the National Science Foundation, Division of Mathematical Sciences (http://www.nsf.gov/) under Agreement DMS. 0931642, the National Cancer Institute (http://www.cancer.gov/) under R01CA138427, and American Cancer Society (http://www.cancer.org/) under RSG-09-188-01-LIB. The funders had no role in study design, data collection and analysis, decision to publish, or preparation of the manuscript.

Competing Interests: The authors have declared that no competing interests exist.

* Email: liao.92@mbi.osu.edu

Introduction

Interleukin-35 (IL-35) is a member of the IL-12 cytokine family. It is produced in human cancer tissues such as in melanoma, B cell lymphoma [1], lung cancer, colon cancer, esophageal carcinoma, hepatocellular carcinoma, cervical carcinoma, and colorectal cancer [2,3], and it plays important roles in tumor progression and tumor immune evasion [1]. $Fox3^+$ regulatory T cells (T_{reg}) are common in tumor microenvironment [4,5], where they induce immune-suppression. They do so by producing various cytokines, including TGF-β, IL-10 [6], and IL-9 [7], thereby promoting tumor growth. It was also shown that T_{reg} secrete IL-35 [8–14]. IL-35 functions through IL-35R on various cell types, and is a potent immune-suppressor. Indeed, T_{reg}-derived IL-35 was shown to inhibit antitumor T cell response [15], whereas IL-35-deficient T_{reg} have significantly reduced activity *in vitro* and *in vivo* [8]. Stable expression of EBI3, a gene that codes for IL-35 subunit, confers growth-promoting activity in lung cancer, whereas small interfering RNA silencing of EBI3 inhibits proliferation of lung cancer [16].

Recently Wang et al. [1] generated IL-35 producing plasmacytoma cancer cells and showed that the expression of IL-35 in tumor microenvironment increased the number of myeloid derived suppressor cells (MDSCs), and promoted tumor angiogenesis; furthermore, IL-35 inhibited the infiltration of cytotoxic T lymphocytes into the tumor microenvironment and rendered the cancer cells less susceptible to CTL destruction.

These experimental results suggest that blocking IL-35 may be an effective therapeutic approach to human cancer. To explore this possibility we develop in the present paper a mathematical model and then conduct *in silica* experiments to evaluate to what extend blocking IL-35 reduces tumor growth.

The model consists of a system of partial differential equations (PDEs) that involve interactions among cells (tumor cells, MDSCs, T cells, T_{reg}s, endothelial cells) and cytokines (M-CSF, TGF-β, VEGF, IL-35). We first consider the situation which corresponds to the experiments in Wang et al. [1]. In these experiments two kinds of plasmacytoma cells were injected into wild type mice: tumor cells that have been transfected with IL-35 (J558-IL-35) so that tumor secretes high amount of IL-35 into the microenvironment, and "normal" plasmacytoma cells (J558-Ctrl) that secrete very small amount of IL-35. There is also a small amount of IL-35 produced by MDSC [17,18] as well as IL-35 produced by T_{reg} [8–14]. We show that the model simulations agree with the experimental data in [1]. We also introduce, in this model, the effect of a drug which inhibits production of IL-35, and simulate various protocols for administering the drug. We find, that administering the drug frequently in small amounts yields better results than administering it infrequently in larger amounts. We also find that the percentage of tumor reduction under anti-IL-35 drug improves when the production of IL-35 by cancer is increased.

Results

Mathematical model

The mathematical model is based on the network schematically shown in Figure 1. Cancer cells secrete M-CSF which attracts MDSCs; cancer cells and MDSCs secrete VEGF which triggers angiogenesis by attracting endothelial cells and enhancing their proliferation. The additional roles of MDSC are described in the caption of Figure 1. In particular, MDSC, inhibits the activation $CD8^+$ T cells via IL-10 and a variety of other mechanisms.

As mentioned in the Introduction, Wang et al. [1] considered two kinds of tumor cells injected into mice: J558-IL-35 and J558-Ctrl. In the case of J558-IL-35, IL-35 is produced mostly by tumor cells, less by T_{reg}, and little by MDSC. In the case of J558-Ctrl, cancer cells produce very small amount of IL-35 so that IL-35 mainly comes from T_{reg} and MDSC. MDSC secretes TGF-β and IL-10 which promote T_{reg} [19,20], and there is a positive feedback loop

$$T_{reg} \rightarrow \text{IL-35} \rightarrow \text{MDSC} \rightarrow T_{reg},$$

where the last activation is activated by TGF-β and IL-10.

We use the network described in Figure 1 to construct a system of partial differential equations. In order to simplify the computations we assume that the tumor and all the variables are radially symmetric. The variables of the model and their dimension are listed below.

$c(r,t)$: tumor cell density, $cell/cm^3$,

$q(r,t)$: M–CSF concentration, pg/cm^3,

$M(r,t)$: Myeloid derived suppressor cell (MDSC) density, $cell/cm^3$,

$I_{35}(r,t)$: Interleukin $-$ 35 concentration, pg/cm^3,

$R(r,t)$: regulatory T cell density, $cell/cm^3$,

$I_\beta(r,t)$: TGF$-\beta$ concentration, pg/cm^3,

$T(r,t)$: T cell density, $cell/cm^3$,

$h(r,t)$: VEGF concentration, pg/cm^3,

$e(r,t)$: endothelial cell (EC) density, $cell/cm^3$,

$w(r,t)$: oxygen concentration, pg/cm^3.

We proceed to write down the differential equation of each of the variables. Most of the parameters are taken from the literatures, as indicated; in Methods we explain how the remaining parameters were estimated.

Tumor cell (c). The density $c(r,t)$ of tumor cells satisfies the following equation:

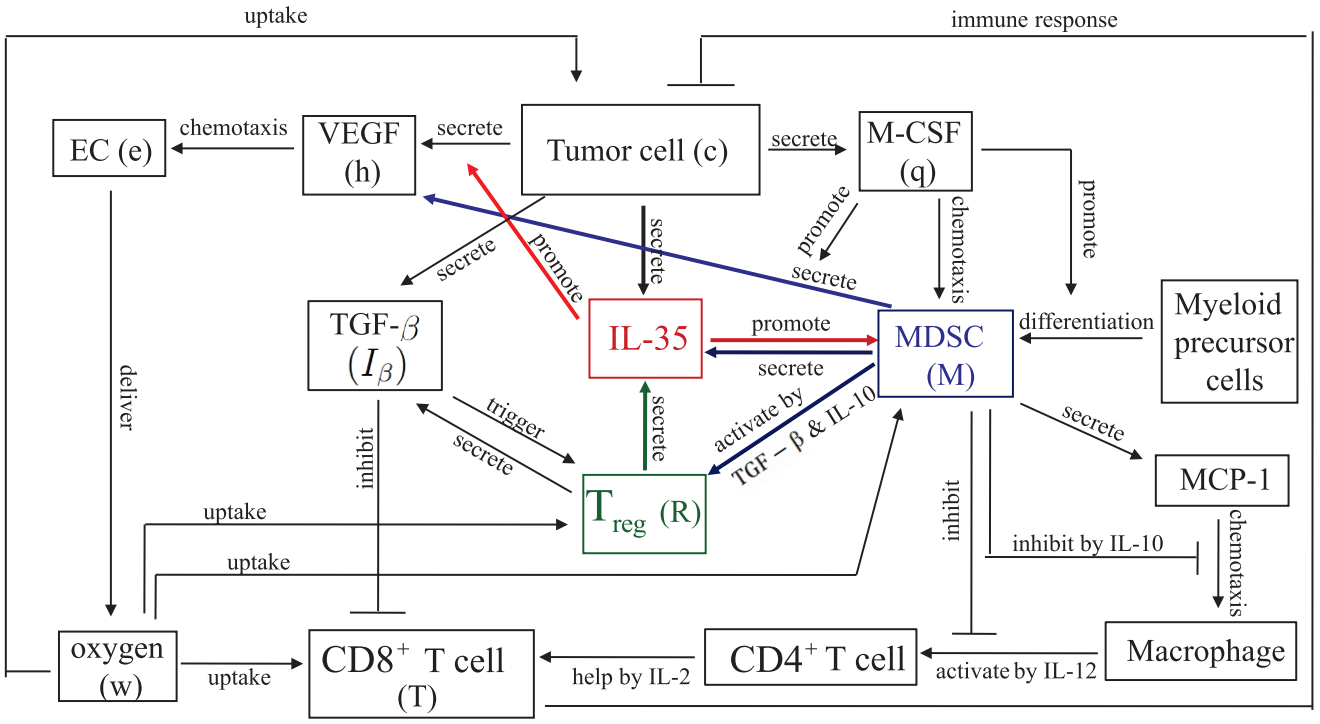

Figure 1. A network showing how IL-35 promotes tumor growth. M-CSF secreted by tumor cells promotes the differentiation of myeloid cells to MDSCs. M-CSF also attracts MDSCs to the tumor microenvironment by chemotaxis and promotes the secretion of VEGF by MDSCs. VEGF secreted by tumor cells and MDSCs attracts endothelial cells to trigger angiogenesis. IL-35 secreted by tumor cells, regulatory T cells and MDSCs promotes the secretion of VEGF by tumor cells and enhances the production of MDSCs. MDSCs promote T_{reg}s, but also secrete MCP-1 to attract macrophages into the tumor microenvironment. Macrophages secrete IL-12 to activate $CD4^+$ T cells, and $CD4^+$ T cells secrete IL-2 which activates $CD8^+$ T cells. MDSCs also produce large amount of IL-10, which inhibits the chemotaxis and activation of $CD4^+$ T cells.
doi:10.1371/journal.pone.0110126.g001

Table 1. Parameters for the tumor cell equation.

Parameter	Description	Dimensional	Reference
D_c	Diffusion coefficient of tumor cells	$4.32\times10^{-6}\ cm^2/day$	[22,25] & estimated
c^*	Carrying capacity of tumor cells	$10^9\ cell/cm^3$	[22,47,55]
μ_c	Apoptosis rate of tumor cell	$4.15\times10^{-1}/day$	[22,66]
η_c	Killing rate of tumor cells from T cells	$3.1574\times10^{-6}\ cm^3/cell/day$	[55,56] & estimated
λ_1	Maximal proliferation rate of tumor cells	$2.5/day$	[22,25,67] & estimated
λ_2	Maximal necrosis rate of tumor cells	$8.3\times10^{-1}/day$	[22,25,55,67]
w_n	Lower bound of oxygen in necrotic	$3.57\times10^7\ pg/cm^3$	[22,68]
w_h	Lower bound of oxygen in extremely hypoxic	$10^8\ pg/cm^3$	[22,55,68]
w_0	Normal oxygen level	$4.65\times10^8\ pg/cm^3$	[22,68]

doi:10.1371/journal.pone.0110126.t001

$$\frac{\partial c}{\partial t}=\underbrace{D_c\frac{1}{r^2}\frac{\partial}{\partial r}(r^2\frac{\partial c}{\partial r})}_{\text{diffusion}}+\underbrace{\lambda_1(w)c(1-\frac{c}{c^*})}_{\text{proliferation}}-\underbrace{\lambda_2(w)c}_{\text{death by necrosis}}-\underbrace{\mu_c c}_{\text{apoptosis}}-\underbrace{\eta_c Tc}_{\text{killed by T cell}}, \tag{1}$$

where

$$\lambda_1(w)=\begin{cases}0 & \text{if } w<w_h,\\ \lambda_1(w-w_h)/(w_0-w_h) & \text{if } w_h\le w\le w_0,\\ \lambda_1 & \text{if } w>w_0,\end{cases}$$

$$\lambda_2(w)=\begin{cases}\lambda_2 & \text{if } w<w_n,\\ \lambda_2(w_h-w)/(w_h-w_n) & \text{if } w_n\le w\le w_h,\\ 0 & \text{if } w>w_h;\end{cases}$$

w_0 is the oxygen level in heathy tissue, and the levels of oxygen for necrotic, extremely hypoxic, and intermediate hypoxic states vary in the intervals $[0,w_n]$, $(w_n,w_h]$ and $(w_h,w_0]$, respectively.

The first term on the right-hand side of Equation (1) represents the dispersion (or diffusion) of tumor cells with diffusion coefficient D_c. The second term accounts for the tumor proliferation, which depends on the concentration of oxygen $w(r,t)$ and tissue carrying capacity c^*. The third and fourth terms represent the death of tumor cells by necrosis and apoptosis, respectively. The last term accounts for the killing of tumor cells by activated $CD8^+$ T cells [21]. The parameters in Equation (1) are listed in Table 1.

M-CSF (q). The concentration of M-CSF is given by the equation:

$$\frac{\partial q}{\partial t}=\underbrace{D_q\frac{1}{r^2}\frac{\partial}{\partial r}(r^2\frac{\partial q}{\partial r})}_{\text{diffusion}}+\underbrace{\alpha_q c}_{\text{production by tumor}}-\underbrace{\mu_q q}_{\text{decay}}. \tag{2}$$

The first term on the right-hand side is the diffusion of M-CSF with coefficient D_q. The second term represents the M-CSF secreted by tumor cells [19,22], and the last term is the decay of M-CSF. The parameters in Equation (2) are listed in Table 2.

Myeloid derived suppressor cell (MDSC) (M). We model the dynamics of the density of MDSC by

$$\frac{\partial M}{\partial t}=\underbrace{\sigma_0}_{\text{source}}+\underbrace{\sigma_1 M_0\times\frac{I_{35}}{I_{35}+c_M}}_{\text{induction of myeloid cells by }I_{35}}+\underbrace{D_M\frac{1}{r^2}\frac{\partial}{\partial r}(r^2\frac{\partial M}{\partial r})}_{\text{diffusion}}-\underbrace{\frac{1}{r^2}\frac{\partial}{\partial r}(r^2k_qM\frac{\partial q}{\partial r})}_{\text{chemotaxis by M-CSF}}+\underbrace{\alpha_M\frac{qM_0}{\sigma_M+q}}_{\text{differentiation from myeloid cells}}-\underbrace{\mu_M M}_{\text{death}}. \tag{3}$$

The first and last terms on the right-hand side account for the source and death of MDSCs. MDSCs undergo dispersion as well as chemotaxis driven by M-CSF (the third and fourth terms) [23–25]. It was reported in [1], that MDSCs do not undergo chemotaxis by IL-35 *in vitro* experiments. However, it has been observed that differentiation of MDSCs from myeloid precursor cells is enhanced by IL-35, although the mechanism is currently unknown [1]. We assume that this mechanism results in the second term on the right-hand side of Equation (3). The fifth term accounts for the differentiation of MDSCs from myeloid cells promoted by M-CSF [26]. The parameters in Equation (3) are listed in Table 3.

IL-35 (I_{35}). The equation for the concentration of IL-35 is the following:

$$\frac{\partial I_{35}}{\partial t}=\underbrace{D_{I_{35}}\frac{1}{r^2}\frac{\partial}{\partial r}(r^2\frac{\partial I_{35}}{\partial r})}_{\text{diffusion}}+\underbrace{\alpha_{35}c}_{\text{production by tumor}}+\underbrace{\beta_{35}R}_{\text{production by }T_{reg}}+\underbrace{\gamma_{35}M}_{\text{production by MDSC}}-\underbrace{\mu_{35}I_{35}}_{\text{decay}}. \tag{4}$$

Experiments indicate that IL-35 can be produced by T_{reg}s [8–14]. IL-35 possesses EBI3 and IL-12p35 subunits [1,11,13,14,27]. In human model, it has been shown that EBI3 was expressed in tumor infiltrating dendritic cells [17,18], which is a subpopulation of MDSCs, and in lung cancer cells [2,3,16], whereas IL-12p35 was detected in $EBI3^+$ tumor cells [17,18]. Hence, cancer cells

Table 2. Parameters for the M-CSF equation.

Parameter	Description	Dimensional	Reference
D_q	Diffusion coefficient of M-CSF	$1.728\times10^{-1}\ cm^2/day$	[22,25,55,69,70]
α_q	Production rate of M-CSF by tumor cell	$2.7648\times10^{-5}\ pg/cell/day$	[22,55,71,72]
μ_q	Decay rate of M-CSF	$4.1472/day$	[22,73]

doi:10.1371/journal.pone.0110126.t002

and MDSCs could be other sources of IL-35 in human and mouse cancer. Accordingly, we include the production of IL-35 by cancer cells (the second term), T_{reg}s (the third term), and MDSCs (the fourth term). For J558-IL-35 mouse model, we take α_{35} large enough and γ_{35} small enough such that, in our simulations, $\alpha_{35}c$ is relatively much larger than $\beta_{35}R$, and $\gamma_{35}M$ is significantly smaller than $\beta_{35}R$. On the other hand, in the J558-Ctrl mouse model, we modify α_{35} to be a much smaller than the value in J558-IL-35 case so that the production of IL-35 by tumor cells is significantly smaller than the productions of IL-35 by T_{reg}s and MDSCs. The parameters in Equation (4) are listed in Table 4.

Regulatory T cell (R). The equation for the density of regulatory T cells is given by

$$\frac{\partial R}{\partial t}=\underbrace{D_R\frac{1}{r^2}\frac{\partial}{\partial r}(r^2\frac{\partial R}{\partial r})}_{\text{diffusion}}+\underbrace{\delta_M\frac{M}{M+\sigma_R}}_{\text{(indirect) activation by MDSC}}+\underbrace{\delta_\beta\frac{I_\beta}{I_\beta+\sigma_\beta}}_{\text{activation by TGF}-\beta}-\underbrace{\mu_R R}_{\text{death}}. \tag{5}$$

T_{reg} is activated by TGF-β (the third term on the right-hand side) and by IL-10. IL-10 is secreted by MDSC [19,20] and, for simplicity, we do not introduce IL-10 explicitly, and represent the activation of T_{reg} by IL-10 by the term $\delta_M M/(M+\sigma_R)$. The parameters in Equation (5) are listed in Table 5.

TGF-β (I_β). The equation for the concentration of TGF-β is the following:

$$\frac{\partial I_\beta}{\partial t}=\underbrace{D_\beta\frac{1}{r^2}\frac{\partial}{\partial r}(r^2\frac{\partial I_\beta}{\partial r})}_{\text{diffusion}}+\underbrace{v_c c}_{\text{production by tumor}}+\underbrace{v_R R}_{\text{production by T}_{reg}}-\underbrace{\mu_\beta I_\beta}_{\text{decay}}. \tag{6}$$

TGF-β is secreted by tumor cells (second term) [28–35] and T_{reg}s (third term) [36–38]. The parameters in Equation (6) are shown in Table 6.

Activated CD8$^+$ T cell (T). Cytotoxic T cells (CTL), or CD8$^+$ T cells, satisfy the equation:

$$\frac{\partial T}{\partial t}=\underbrace{D_T\frac{1}{r^2}\frac{\partial}{\partial r}(r^2\frac{\partial T}{\partial r})}_{\text{diffusion}}+\underbrace{\frac{s_M}{s_M+a_1M}}_{\text{inhibition}}\times\left[-\underbrace{\frac{1}{r^2}\frac{\partial}{\partial r}(r^2\beta_1T\frac{\partial(a_2M)}{\partial r})}_{\text{(indirect) chemotaxis by MCP}-1}+\underbrace{\frac{\beta_2(a_3M)}{(a_3M)+c_5}}_{\text{(indirect) activation}}\times\underbrace{\frac{s_\beta}{s_\beta+I_\beta}}_{\text{inhibit by }I_\beta}\right]-\underbrace{\mu_T T}_{\text{death}}. \tag{7}$$

MDSC secretes MCP-1 which exerts chemotactic force on macrophages [39,40], while macrophages secrete IL-12 which

Table 3. Parameters for the MDSC equation.

Parameter	Description	Dimensional	Reference
σ_0	Source of MDSC	$1.10345\times10^5\ cell/cm^3/day$	[56,58] & estimated
σ_1	Maximal production rate via I_{35}	$4.65518\times10^2/day$	[1] & estimated
c_M		$10^5\ pg/cm^3$	estimated
D_M	Diffusion coefficient of MDSC	$4.32\times10^{-6}\ cm^2/day$	[22,25] & estimated
k_q	Chemotaxis rate of MDSC for M-CSF	$5.2\times10^{-7}\ cm^5/pg/day$	[25,55]
α_M	Polarization rate of MDSC by M-CSF	$7.5\times10^{-1}/day$	[56] & estimated
M_0	Density of myeloid precursor cells	$8\times10^3\ cell/cm^3$	[56,58]
σ_M		$7.5\times10\ pg/cm^3$	[56,58]
μ_M	Death rate of MDSC	$3\times10^{-2}/day$	[58,59]

doi:10.1371/journal.pone.0110126.t003

Table 4. Parameters for the IL-35 equation.

Parameter	Description	Dimensional	Reference
$D_{I_{35}}$	Diffusion coefficient of I_{35}	$1.25\times10^{-3}\ cm^2/day$	[60] & estimated
α_{35}	Production rate of I_{35} from tumor	$10^{-3}\ pg/cell/day$ for J558-IL-35 mouse	[1,16–18] & estimated
α_{35}	Production rate of I_{35} from tumor	$10^{-7}\ pg/cell/day$ for J558-Ctrl mouse	[1] & estimated
β_{35}	Production rate of I_{35} from T_{reg}	$1.67\times10^{-3}\ pg/cell/day$	[34] & estimated
γ_{35}	Production rate of I_{35} from MDSC	$10^{-4}\ pg/cell/day$	[17,18] & estimated
μ_{35}	Decay rate of I_{35}	$2/day$	[61–63] & estimated

doi:10.1371/journal.pone.0110126.t004

activates $CD4^+$ T cells [41] and $CD4^+$ T cells produce IL-2 [42,43] which activates $CD8^+$ T cells. The activation of $CD8^+$ T cells is inhibited by TGF-β [44–46]. For simplicity we combine all these process by attributing the chemotactic force or $CD8^+$ T cells and activation source of $CD8^+$ T cells to MDSC (the terms in square brackets in Equation (7)). The factor $s_M/(s_M+a_1M)$ represents the fact that MDSC suppresses $CD8^+$ T cells proliferation by amino acid metabolism. The parameters in Equation (7) are listed in Table 7.

VEGF (h). The concentration of VEGF evolves according to the equation

$$\frac{\partial h}{\partial t}=\underbrace{D_h\frac{1}{r^2}\frac{\partial}{\partial r}(r^2\frac{\partial h}{\partial r})}_{\text{diffusion}}+\underbrace{\lambda_5(w)c\times\frac{I_{35}+k_1}{I_{35}+\sigma_h}}_{\text{production by tumor promoted by }I_{35}}+\underbrace{\lambda_6(w)M\times\frac{q+k_2}{q+q_0}}_{\text{production by MDSC}}-\underbrace{\mu_h h}_{\text{decay}}, \tag{8}$$

where $\lambda_5(w)=\lambda_5\phi(w)$ and $\lambda_6(w)=\lambda_6\phi(w)$ depend on the oxygen concentration w, as follows:

$$\phi(w)=\begin{cases}0 & \text{if } w<w_n,\\ \dfrac{\exp(10(w-w_n))-1}{\exp(10(w^*-w_n))-1} & \text{if } w_n\le w<w^*,\\ 1-0.7(w-w^*)/(w_0-w^*) & \text{if } w^*\le w\le w_0,\\ 0.3 & \text{if } w>w_0,\end{cases}$$

and $w^*\in(w_h,w_0)$ is the threshold at which the hypoxic effect on VEGF production by tumor cells and MDSCs is maximal. The function $\phi(w)$ is chosen such that tumor cells and MDSCs can secrete VEGF under mild hypoxic conditions. The second term on the right-hand side of Equation (8) represents the VEGF produced by tumor cells and enhanced by I_{35} [1], and the third term accounts for VEGF produced by MDSCs and enhanced by M-CSF [47]; accordingly, the ratios k_1/σ_h and k_2/q_0 should be small. The parameters in Equation (8) are listed in Table 8.

Endothelial cell (EC) (e). The equation of the density of EC includes dispersion, chemotaxis by VEGF, and proliferation by VEGF:

$$\frac{\partial e}{\partial t}=\underbrace{D_e\frac{1}{r^2}\frac{\partial}{\partial r}(r^2\frac{\partial e}{\partial r})}_{\text{diffusion}}-\underbrace{\frac{1}{r^2}\frac{\partial}{\partial r}(r^2k_he\frac{\partial h}{\partial r})}_{\text{chemotaxis by VEGF}}+\underbrace{\lambda_{12}e(1-\frac{e}{e_1})\frac{h-h_1}{h_0}H(h-h_1)}_{\text{proliferation}}. \tag{9}$$

Here e_1 is the maximal density of EC inside the tumor, and $H(\cdot)$ is defined by

$$H(h-h_1)=\begin{cases}1 \text{ if } h\ge h_1\\ 0 \text{ if } h<h_1.\end{cases}$$

The last term, taken from [22], reflects the fact that VEGF induces proliferation of EC when the concentration of VEGF is higher than the threshold h_1. The parameters in Equation (9) are given in Table 9.

Oxygen (w). We model the concentration of oxygen by the equation:

Table 5. Parameters for the T_{reg} equation.

Parameter	Description	Dimensional	Reference
D_R	Diffusion coefficient of T_{reg}	$4.32\times10^{-6}\ cm^2/day$	[22,25] & estimated
δ_M	Maximal activation rate of T_{reg} by MDSC	$1.25\times10^6\ cell/cm^3/day$	estimated
σ_R		$10^7\ cell/cm^3$	estimated
δ_β	Maximal activation rate of T_{reg} by TGF-β	$3.327\times10^6\ cell/cm^3/day$	[38] & estimated
σ_β		$2.4\times10^3\ pg/cm^3$	[38,64] & estimated
μ_R	Death rate of T_{reg}	$10^{-1}/day$	[34,74,75]

doi:10.1371/journal.pone.0110126.t005

Table 6. Parameters for the TGF-β equation.

Parameter	Description	Dimensional	Reference
D_β	Diffusion coefficient of I_β	$8.64\times10^{-2}\ cm^2/day$	[76]
v_c	Production rate of I_β by tumor cells	$5.5\times10^{-6}\ pg/cell/day$	[34] & estimated
v_R	Production rate of I_β by T_{reg}s	$9\times10^{-7}\ pg/cell/day$	[34] & estimated
μ_β	Decay rate of I_β	$0.693/day$	[76]

doi:10.1371/journal.pone.0110126.t006

$$\frac{\partial w}{\partial t} = \underbrace{\lambda_7 e}_{\text{delivered by EC}} + \underbrace{D_w \frac{1}{r^2}\frac{\partial}{\partial r}(r^2\frac{\partial w}{\partial r})}_{\text{diffusion}} - \underbrace{\lambda_8 Tw}_{\text{uptake by CD8}^+\text{ T cell}} - \underbrace{\lambda_9 Mw}_{\text{uptake by MDSC}} - \underbrace{\lambda_{10} Rw}_{\text{uptake by T}_{reg}} - \underbrace{\lambda_{11} cw}_{\text{uptake by tumor}} . \quad (10)$$

Oxygen is delivered by EC (the first term) and is taken up by $CD8^+$ T cells (the third term), MDSCs (the fourth term), T_{reg}s (the fifth term), and tumor cells (the last term). The parameters in Equation (10) are listed in Table 10.

We assume that the tumor is radially symmetric and is contained in a sphere $0\le r\le L$, where $L=1.5\ cm$.

We next introduce the initial and boundary conditions for each of the variables.

Initial conditions. We assume that the tumor cells are concentrated initially near $r=0$, and take

$$c(r,0)=\begin{cases} c_0(e^{-r/\epsilon}-e^{-L_0/\epsilon}) & \text{if } 0\le r\le L_0 \\ 0 & \text{if } L_0<r\le L, \end{cases} \quad (11)$$

with a positive parameter ϵ, $0<\epsilon\le1$, and scaling parameters $c_0=7.2\times10^8\ cell/cm^3$ and $L_0=0.5\ cm$. Since M-CSF is secreted by tumor cells, we take the initial concentration of M-CSF to be similar to the density of tumor cells,

$$q(r,0)=\begin{cases} \frac{\alpha_q}{\mu_q}c_0(e^{-r/\epsilon}-e^{-L_0/\epsilon}) & \text{if } 0\le r\le L_0 \\ 0 & \text{if } L_0<r\le L, \end{cases}$$

where the constant α_q/μ_q comes from the steady state equation for q.

Since tumor cells are concentrated at the center $r=0$, we assume that the MDSC is higher at the center and negligible near the boundary $r=L$,

$$M(r,0)=\begin{cases} \frac{\sigma_0}{\mu_M}(e^{-r/\epsilon}-e^{-L_0/\epsilon}) & \text{if } 0\le r\le L_0 \\ 0 & \text{if } L_0<r\le L, \end{cases}$$

where the constant σ_0/μ_M comes from the steady state equation of Equation (3). We assume that initially there are no activated $CD8^+$ T cells, and take

$$T(r,0)=0 \text{ if } 0\le r\le L.$$

The activation of T_{reg}s and the productions of I_{35} and VEGF are triggered by tumor cells and MDSCs; accordingly, we take

$$R(r,0)=\begin{cases} \frac{\delta_M+\delta_\beta}{\mu_R}(e^{-r/\epsilon}-e^{-L_0/\epsilon}) & \text{if } 0\le r\le L_0 \\ 0 & \text{if } L_0<r\le L, \end{cases}$$

$$I_{35}(r,0)=\begin{cases} I_{35}^0(e^{-r/\epsilon}-e^{-L_0/\epsilon}) & \text{if } 0\le r\le L_0 \\ 0 & \text{if } L_0<r\le L, \end{cases}$$

$$h(r,0)=\begin{cases} h_0(e^{-r/\epsilon}-e^{-L_0/\epsilon}) & \text{if } 0\le r\le L_0 \\ 0 & \text{if } L_0<r\le L, \end{cases}$$

and $I_{35}^0=10^2\ pg/cm^3$, and $h_0=10^3\ pg/cm^3$. Similarly, I_β is produced by tumor cells and T_{reg}s, so accordingly we take

$$I_\beta(r,0)=\begin{cases} I_\beta^0(e^{-r/\epsilon}-e^{-L_0/\epsilon}) & \text{if } 0\le r\le L_0 \\ 0 & \text{if } L_0<r\le L, \end{cases}$$

where $I_\beta^0=2.4\times10^3\ pg/cm^3$.

Endothelial cells migrate into the tumor from the surrounding normal healthy tissue, so we take

$$e(r,0)=\begin{cases} e_0e^{-(L_0-r)/\epsilon} & \text{if } 0\le r\le L_0 \\ e_0 & \text{if } L_0<r\le L, \end{cases}$$

where e_0 is the density of endothelial cell in normal healthy tissue. Finally, since endothelial cells represent capillaries through which oxygen is delivered, we prescribe

$$w(r,0)=\begin{cases} w_0e^{-(L_0-r)/\epsilon} & \text{if } 0\le r\le L_0 \\ w_0 & \text{if } L_0<r\le L, \end{cases}$$

where w_0 is the oxygen concentration in normal healthy tissue.

Boundary conditions. Since we assume radial symmetry, the first r-derivative of each variable vanishes at $r=0$. We assume no-flux condition at $r=L$ for all the variables except for the oxygen and endothelial cells, and we take

Table 7. Parameters for the $CD8^+$ T equation.

Parameter	Description	Dimensional	Reference
D_T	Diffusion coefficient of T cells	$4.32\times10^{-6}\ cm^2/day$	[22,25] & estimated
s_M		$5\times10^{6}\ pg/cm^3$	[58,77] & estimated
β_1	Chemotaxis rate of T cell from MCP-1	$8.64\times10^{-9}\ cm^5/pg/day$	[78–80] & estimated
β_2	Activation rate from IL-12	$2.5\times10^{5}\ cell/cm^3/day$	[58,77] & estimated
a_1	Production rate of IL-10 by MDSC	$2\ pg/cell$	estimated
a_2	Chemotaxis rate of MCP-1 by MDSC	$10^{-2}\ pg/cell$	estimated
a_3	Production rate of IL-12 by MDSC	$10^{-2}\ pg/cell$	estimated
c_5		$7.5\times10\ pg/cm^3$	[56,77] & estimated
s_β		$2.9\times10^{3}\ pg/cm^3$	[34] & estimated
μ_T	Death rate of T cells	$3\times10^{-1}/day$	[58,81–85]

doi:10.1371/journal.pone.0110126.t007

$$\begin{aligned}\frac{\partial w}{\partial r}+\mu(w-w_0)&=0 \text{ at } r=L,\\ \frac{\partial e}{\partial r}+\mu(e-e_0)&=0 \text{ at } r=L\end{aligned}\qquad(12)$$

where μ is the flux rate of EC from healthy normal tissue into the tumor microenvironment.

Parameters nondimensionalization.. We nondimensionalizate the Equations (1)–(10) by the following scaling:

$$\hat{r}=r/L_0,\ \hat{t}=t/\tau,$$

$$\hat{c}=c/c_0,\ \hat{q}=q/q_0,\ \hat{M}=M/M^0,\ \hat{I}_{35}=I_{35}/I^0_{35},\ \hat{R}=R/R_0,$$

$$\hat{T}=T/T_0,\ \hat{h}=h/h_0,\ \hat{e}=e/e_0,\ \hat{w}=w/w_0,$$

$$\{\hat{D}_c,\hat{D}_q,\hat{D}_M,\hat{D}_{I_{35}},\hat{D}_R,\hat{D}_\beta,\hat{D}_T,\hat{D}_h,\hat{D}_e,\hat{D}_w\}$$

$$=\frac{\tau}{L_0^2}\{D_c,D_q,D_M,D_{I_{35}},D_R,D_\beta,D_T,D_h,D_e,D_w\},$$

$$\{\hat{\mu}_c,\hat{\mu}_q,\hat{\mu}_M,\hat{\mu}_{35},\hat{\mu}_R,\hat{\mu}_\beta,\hat{\mu}_T,\hat{\mu}_h\}=\tau\{\mu_c,\mu_q,\mu_M,\mu_{35},\mu_R,\mu_\beta,\mu_T,\mu_h\},$$

$$\{\hat{\alpha}_q,\hat{\alpha}_M,\hat{\alpha}_{35}\}=\tau\{c_0\alpha_q/q_0,\alpha_M,c_0\alpha_{35}/I^0_{35}\},$$

$$\{\hat{\beta}_{35},\hat{\gamma}_{35}\}=\tau\{R_0\beta_{35}/I^0_{35},M^0\gamma_{35}/I^0_{35}\},\{\hat{k}_q,\hat{k}_h\}=\frac{\tau}{L_0^2}\{q_0k_q,h_0k_h\},$$

$$\{\hat{\delta}_M,\hat{\delta}_\beta\}=\tau\{\delta_M/R_0,\delta_\beta/R_0\},\{\hat{v}_c,\hat{v}_R\}=\tau\{c_0v_c/I^0_\beta,R_0v_R/I^0_\beta\},$$

Table 8. Parameters for the VEGF equation.

Parameter	Description	Dimensional	Reference
D_h	Diffusion coefficient of VEGF	$8.64\times10^{-2}\ cm^2/day$	[22,55,86,87]
k_1		$3.7\times10^{2}\ pg/cm^3$	estimated
σ_h	Critical value of I_{35}	$3.7\times10^{5}\ pg/cm^3$	estimated
q_0	Critical value of M-CSF	$10^{3}\ pg/cm^3$	[22,55]
k_2		$q_0/100=10\ pg/cm^3$	estimated
μ_h	Decay rate of VEGF	$1.08864\times10/day$	[22,57]
λ_5		$2.86\times10^{-4}\ pg/cell/day$	[22,55] & estimated
λ_6		$1.58\times10^{-3}\ pg/cell/day$	[22,55]
w^*		$4.185\times10^{8}\ pg/cm^3$	[22,55] & estimated

doi:10.1371/journal.pone.0110126.t008

Table 9. Parameters for the EC equation.

Parameter	Description	Dimensional	Reference
D_e	Diffusion coefficient of EC	$4.32\times10^{-6}\ cm^2/day$	[22,25,57] & estimated
k_h	Chemotaxis force of EC by VEGF	$4.1472\times10^{-7}\ cm^5/pg/day$	[22,87] & estimated
λ_{12}	Proliferation rate by VEGF	$5.83\times10^{-1}/day$	[88] & estimated
e_1	Maximal density of EC inside the tumor	$7.5\times10^{6}\ cell/cm^3$	[22] & estimated
h_0	Scaling parameter for VEGF	$10^3\ pg/cm^3$	[89] & estimated
h_1	Threshold concentration of VEGF	$1.48\times10^{3}\ pg/cm^3$	[90] & estimated

doi:10.1371/journal.pone.0110126.t009

$$\{\hat{\lambda}_1(\hat{w}),\hat{\lambda}_2(\hat{w}),\hat{\lambda}_5(\hat{w}),\hat{\lambda}_6(\hat{w})\}=\tau\{\lambda_1(w),\lambda_2(w),c_0\lambda_5(w)/h_0,M^0\lambda_6(w)/h_0\},$$

$$\{\hat{\lambda}_7,\hat{\lambda}_8,\hat{\lambda}_9,\hat{\lambda}_{10},\hat{\lambda}_{11},\hat{\lambda}_{12}\}=\tau\{e_0\lambda_7/w_0,T_0\lambda_8,M^0\lambda_9,R_0\lambda_{10},c_0\lambda_{11},\lambda_{12}\},$$

$$\hat{\sigma}_0=\tau\sigma_0/M^0,\ \hat{\sigma}_1=\tau\sigma_1,\ \hat{\sigma}_h=\sigma_h/I_{35}^0,\ \hat{\sigma}_M=\sigma_M/q_0,\ \hat{\sigma}_R=\sigma_R/M^0,\ \hat{\sigma}_\beta=\sigma_\beta/I_\beta^0,$$

$$\hat{\beta}_1=M^0\tau\beta_1/L_0^2,\ \hat{\beta}_2=\tau\beta_2/T_0,\ \hat{\gamma}_{35}=\tau M^0\gamma_{35}/I_{35}^0,\ \hat{\eta}_c=T_0\tau\eta_c,$$

$$\hat{a}_1=1,\ \hat{a}_2=1,\ \hat{a}_3=0.01,\ \hat{c}^*=c^*/c_0,\ \hat{c}_5=c_5/M^0,\ \hat{c}_M=c_M/I_{35}^0,\ \hat{M}_0=1,$$

$$\hat{k}_1=k_1/I_{35}^0,\ \hat{k}_2=k_2/q_0,\ \hat{e}_1=e_1/e_0,\ \hat{h}_1=h_1/h_0,\ \hat{s}_M=s_M/M^0,\ \hat{s}_\beta=s_\beta/I_\beta^0,$$

where the scaling parameters are

$$L_0=0.5\ cm,\tau=3\ days,$$

$$c_0=7.2\times10^8\ cell/cm^3,\ T_0=R_0=\ 10^5\ cell/cm^3,\ M^0=2\times10^8\ cell/cm^3,$$

$$e_0=2.5\times10^6\ cell/cm^3,\ w_0=4.65\times10^8\ pg/cm^3,$$

$$q_0=h_0=10^3\ pg/cm^3,\ I_{35}^0=10^2\ pg/cm^3,\ I_\beta^0=2.4\times10^3\ pg/cm^3.$$

The dimensional and nondimensional values of all the parameters of Tables 1–10 are summarized in Tables 11 and 12.

After dropping the symbol "^", the model equations in the nondimensional form are as follows:

Numerical simulation

In accordance with the experiments in Wang et al. [1], we consider two types of mice plasmacytoma J558 cells in wild type mice:

(i) J558-Ctrl tumor cells that secrete a very small amount of I_{35}.

(ii) J558-IL-35 tumor cells that secrete a large amount of I_{35}.

We use matlab with $dr=1/40$ and $dt=7/216000$ in nondimensional variables (i.e., $dr=1/80\ cm$ and $dt=7/72000\ day$ in dimensional variables). Figure 2 displays the spatial distributions of tumor cell density in cases (i)–(ii) at different times. We note that, in Figure 2, as time goes on, tumor cells migrate toward the boundary $r=1.5\ cm$, where oxygen is rich while tumor cell density is lower near the center $r=0\ cm$, where oxygen is sparse. The migration speeds of these two cases (i)–(ii) are similar to each other, but tumor cells with larger I_{35} production (i.e., J558-IL-35 case) have higher peak during migration.

Table 10. Parameters for the oxygen equation.

Parameter	Description	Dimensional	Reference
λ_7	Delivery rate of oxygen	$6.3936\times10^2\ pg/cell/day$	[55]
D_w	Diffusion coefficient of oxygen	$4.32\times10^{-2}\ cm^2/day$	[25,55,69,87]
λ_8	Consumption rate by T cells	$1.61568\times10^{-8}\ cm^3/cell/day$	[55,65] & estimated
λ_9	Consumption rate by MDSC	$1.61568\times10^{-8}\ cm^3/cell/day$	[55,56,65] & estimated
λ_{10}	Consumption rate by T_{reg}	$1.61568\times10^{-8}\ cm^3/cell/day$	[55,65] & estimated
λ_{11}	Consumption rate by tumor cells	$1.728\times10^{-8}\ cm^3/cell/day$	[55,91,92]

doi:10.1371/journal.pone.0110126.t010

The results of Wang et al. [1] were reported 2 weeks after injection of tumor cells into mice. Hence, we compare our simulations at the end of the second week with the results in [1]. In Figure 3(C), the ratio for MDSC of J558-IL-35 to J558-Ctrl is 2, combining these results (Figures seven B, seven D, and seven E in [1]), we find that this ratio (for $T_{reg}/CD8^+$ T cells) is 0.54. From our Figures 3(E) and 3(H), we compute the ratio of J558-IL-35 to J558-Ctrl to be 0.56. Thus in all the above three cases we get a

$$
\begin{cases}
\frac{\partial c}{\partial t} = \underbrace{D_c\frac{1}{r^2}\frac{\partial}{\partial r}(r^2\frac{\partial c}{\partial r})}_{\text{diffusion}} + \underbrace{\lambda_1(w)c(1-\frac{c}{c^*})}_{\text{proliferation}} - \underbrace{\lambda_2(w)c}_{\text{death by necrosis}} - \underbrace{\mu_c c}_{\text{apoptosis}} - \underbrace{\eta_c T c}_{\text{killed by T cell}} \\
\frac{\partial q}{\partial t} = \underbrace{D_q\frac{1}{r^2}\frac{\partial}{\partial r}(r^2\frac{\partial q}{\partial r})}_{\text{diffusion}} + \underbrace{\alpha_q c}_{\text{production by tumor}} - \underbrace{\mu_q q}_{\text{decay}} \\
\frac{\partial M}{\partial t} = \underbrace{\sigma_0}_{\text{source}} + \underbrace{\sigma_1 M_0 \times \frac{I_{35}}{I_{35}+c_M}}_{\text{induction of myeloid cells by } I_{35}} + \underbrace{D_M\frac{1}{r^2}\frac{\partial}{\partial r}(r^2\frac{\partial M}{\partial r})}_{\text{diffusion}} - \underbrace{\frac{1}{r^2}\frac{\partial}{\partial r}(r^2 k_q M\frac{\partial q}{\partial r})}_{\text{chemotaxis by M-CSF}} \\
\qquad + \underbrace{\alpha_M\frac{qM_0}{\sigma_M+q}}_{\text{differentiation from myeloid cells}} - \underbrace{\mu_M M}_{\text{death}} \\
\frac{\partial I_{35}}{\partial t} = \underbrace{D_{I_{35}}\frac{1}{r^2}\frac{\partial}{\partial r}(r^2\frac{\partial I_{35}}{\partial r})}_{\text{diffusion}} + \underbrace{\alpha_{35}c}_{\text{production by tumor}} + \underbrace{\beta_{35}R}_{\text{production by T}_{reg}} + \underbrace{\gamma_{35}M}_{\text{production by MDSC}} - \underbrace{\mu_{35}I_{35}}_{\text{decay}} \\
\frac{\partial R}{\partial t} = \underbrace{D_R\frac{1}{r^2}\frac{\partial}{\partial r}(r^2\frac{\partial R}{\partial r})}_{\text{diffusion}} + \underbrace{\delta_M\frac{M}{M+\sigma_R}}_{\text{(indirect) activation by MDSC}} + \underbrace{\delta_\beta\frac{I_\beta}{I_\beta+\sigma_\beta}}_{\text{activation by TGF-}\beta} - \underbrace{\mu_R R}_{\text{death}} \\
\frac{\partial I_\beta}{\partial t} = \underbrace{D_\beta\frac{1}{r^2}\frac{\partial}{\partial r}(r^2\frac{\partial I_\beta}{\partial r})}_{\text{diffusion}} + \underbrace{\nu_c c}_{\text{production by tumor}} + \underbrace{\nu_R R}_{\text{production by T}_{reg}} - \underbrace{\mu_\beta I_\beta}_{\text{decay}} \\
\frac{\partial T}{\partial t} = \underbrace{D_T\frac{1}{r^2}\frac{\partial}{\partial r}(r^2\frac{\partial T}{\partial r})}_{\text{diffusion}} + \underbrace{\frac{s_M}{s_M+a_1 M}}_{\text{inhibition}} \times [- \underbrace{\frac{1}{r^2}\frac{\partial}{\partial r}(r^2\beta_1 T\frac{\partial(a_2 M)}{\partial r})}_{\text{(indirect) chemotaxis by MCP}-1} + \underbrace{\frac{\beta_2(a_3 M)}{(a_3 M)+c_5}}_{\text{(indirect) activation}} \times \underbrace{\frac{s_\beta}{s_\beta+I_\beta}}_{\text{inhibit by } I_\beta}] \\
\qquad - \underbrace{\mu_T T}_{\text{death}} \\
\frac{\partial h}{\partial t} = \underbrace{D_h\frac{1}{r^2}\frac{\partial}{\partial r}(r^2\frac{\partial h}{\partial r})}_{\text{diffusion}} + \underbrace{\lambda_5(w)c\times\frac{I_{35}+k_1}{I_{35}+\sigma_h}}_{\text{production by tumor promoted by I}_{35}} + \underbrace{\lambda_6(w)M\times\frac{q+k_2}{q+1}}_{\text{production by MDSC}} - \underbrace{\mu_h h}_{\text{decay}} \\
\frac{\partial e}{\partial t} = \underbrace{D_e\frac{1}{r^2}\frac{\partial}{\partial r}(r^2\frac{\partial e}{\partial r})}_{\text{diffusion}} - \underbrace{\frac{1}{r^2}\frac{\partial}{\partial r}(r^2 k_h e\frac{\partial h}{\partial r})}_{\text{chemotaxis by VEGF}} + \underbrace{\lambda_{12}e(1-\frac{e}{e_1})(h-h_1)H(h-h_1)}_{\text{proliferation}} \\
\frac{\partial w}{\partial t} = \underbrace{\lambda_7 e}_{\text{delivered by EC}} + \underbrace{D_w\frac{1}{r^2}\frac{\partial}{\partial r}(r^2\frac{\partial w}{\partial r})}_{\text{diffusion}} - \underbrace{\lambda_8 T w}_{\text{uptake by CD8}^+\text{ T cell}} - \underbrace{\lambda_9 M w}_{\text{uptake by MDSC}} - \underbrace{\lambda_{10}R w}_{\text{uptake by T}_{reg}} \\
\qquad - \underbrace{\lambda_{11}c w}_{\text{uptake by tumor}} .
\end{cases}
\tag{13}
$$

which is the same as Figure five A in [1]. In Figure 3(H), the ratio for VEGF of J558-IL-35 to J558-Ctrl is 17, which is the approximately same as Figure four D in [1]. Next, we compare the ratio for $T_{reg}/CD8^+$ T cells of J558-IL-35 to J558-Ctrl with the result in [1]. But, in [1], they only showed the percentages of $CD8^+/CD45^+$, of $CD4^+/CD45^+$, and of $Foxp3^+/CD4^+$. By very good quantitative fit with the experimental results of Wang et al. [1]. Finally, from Figure 3(A), we see that for tumor cells the ratio of J558-IL-35 to J558-Ctrl is 2.4, which is somewhat less than the ratio for the tumor volume of B16-IL-35 mice to B16-Ctrl mice in Figure three F in [1], and significantly less for J558-IL-35 mice. This discrepancy may be explained by the fact that *in vivo* the

Table 11. Model parameters and units.

Parameter	Dimensional	Dimensionless
D_c	$4.32\times10^{-6}\ cm^2/day$	5.184×10^{-5}
D_q	$1.728\times10^{-1}\ cm^2/day$	2.0736
D_M	$4.32\times10^{-6}\ cm^2/day$	5.184×10^{-5}
$D_{I_{35}}$	$1.25\times10^{-3}\ cm^2/day$	1.5×10^{-2}
D_R	$4.32\times10^{-6}\ cm^2/day$	5.184×10^{-5}
D_β	$8.64\times10^{-2}\ cm^2/day$	1.0368
D_T	$4.32\times10^{-6}\ cm^2/day$	5.184×10^{-5}
D_h	$8.64\times10^{-2}\ cm^2/day$	1.0368
D_e	$4.32\times10^{-6}\ cm^2/day$	5.184×10^{-5}
D_w	$4.32\times10^{-2}\ cm^2/day$	5.184×10^{-1}
α_q	$2.7648\times10^{-5}\ pg/cell/day$	5.97197×10
α_M	$7.5\times10^{-1}/day$	2.25
α_{35}	$10^{-3}\ pg/cell/day$ for J558-IL-35 mouse	2.16×10^4 for J558-IL-35 mouse
α_{35}	$10^{-7}\ pg/cell/day$ for J558-Ctrl mouse	2.16 for J558-Ctrl mouse
β_{35}	$1.67\times10^{-3}\ pg/cell/day$	5
γ_{35}	$10^{-4}\ pg/cell/day$	6×10^2
δ_M	$1.25\times10^6\ cell/cm^3/day$	3.75×10
δ_β	$3.327\times10^6\ cell/cm^3/day$	99.81
η_c	$3.1574\times10^{-6}\ cm^3/cell/day$	9.47232×10^{-1}
σ_0	$5.51725\times10^4\ cell/cm^3/day$	8.2759×10^{-4}
σ_1	$4.65518\times10^2/day$	1.39655×10^3
σ_M	$7.5\times10\ pg/cm^3$	7.5×10^{-2}
σ_R	$10^7\ cell/cm^3$	5×10^{-2}
σ_β	$2.4\times10^3\ pg/cm^3$	1
σ_h	$3.7\times10^5\ pg/cm^3$	3.7×10^3
λ_1	$2.5/day$	7.5
λ_2	$8.3\times10^{-1}/day$	2.49
λ_5	$2.86\times10^{-4}\ pg/cell/day$	6.1776×10^2
λ_6	$1.58\times10^{-3}\ pg/cell/day$	9.48×10^2
λ_7	$6.3936\times10^2\ pg/cell/day$	1.03123×10
λ_8	$1.61568\times10^{-8}\ cm^3/cell/day$	4.84704×10^{-3}
λ_9	$1.61568\times10^{-8}\ cm^3/cell/day$	9.69408
λ_{10}	$1.61568\times10^{-8}\ cm^3/cell/day$	4.84704×10^{-3}
λ_{11}	$1.728\times10^{-8}\ cm^3/cell/day$	3.73248×10
λ_{12}	$5.83\times10^{-1}/day$	1.75
v_c	$5.5\times10^{-6}\ pg/cell/day$	4.95
v_R	$9\times10^{-7}\ pg/cell/day$	1.125×10^{-4}
ϵ	1	1
μ_c	$4.15\times10^{-1}/day$	1.245
μ_q	$4.1472/day$	1.24416×10
μ_M	$3\times10^{-2}/day$	9×10^{-2}
μ_{35}	$2/day$	6
μ_R	$10^{-1}/day$	3×10^{-1}
μ_β	$0.693/day$	2.079
μ_T	$3\times10^{-1}/day$	9×10^{-1}
μ_h	$1.08864\times10/day$	3.26592×10
μ	$10/cm$	5

doi:10.1371/journal.pone.0110126.t011

Table 12. Model parameters and units.

Parameter	Dimensional	Dimensionless
c^*	$10^9\ cell/cm^3$	1.38889(1.39)
c_M	$10^5\ pg/cm^3$	10^3
k_1	$3.7\times10^2\ pg/cm^3$	3.7
k_2	$10\ pg/cm^3$	10^{-2}
k_h	$4.1472\times10^{-7}\ cm^5/pg/day$	4.97664×10^{-3}
k_q	$5.2\times10^{-7}\ cm^5/pg/day$	6.24×10^{-3}
M_0	$8\times10^3\ cell/cm^3$	4×10^{-5}
s_M	$5\times10^6\ cell/cm^3$	2.5×10^{-2}
s_β	$2.9\times10^3\ pg/cm^3$	1.20833
w_n	$3.57\times10^{-7}\ pg/cm^3$	7.68×10^{-2}
w_h	$10^8\ pg/cm^3$	2.15×10^{-1}
w_*	$4.185\times10^8\ pg/cm^3$	9×10^{-1}
β_1	$8.64\times10^{-9}\ cm^5/pg/day$	2.0736×10
β_2	$2.5\times10^5\ cell/cm^3/day$	7.5
a_1	$2\ pg/cell$	2
a_2	$10^{-2}\ pg/cell$	10^{-2}
a_3	$10^{-2}\ pg/cell$	10^{-2}
c_5	$7.5\times10\ pg/cm^3$	3.75×10^{-7}
e_1	$7.5\times10^6\ cell/cm^3$	3
h_1	$1.48\times10^3\ pg/cm^3$	1.48
a	$2.25\ cm^2$	9
L_0	$5\times10^{-1}\ cm$	1
L	$1.5\ cm$	3
τ	$3\ days$	1
c_0	$7.2\times10^8\ cell/cm^3$	1
q_0	$10^3\ pg/cm^3$	1
M^0	$2\times10^8\ cell/cm^3$	1
I_{35}^0	$10^2\ pg/cm^3$	1
R_0	$10^5\ cell/cm^3$	1
I_β^0	$2.4\times10^3\ pg/cm^3$	1
T_0	$10^5\ cell/c,^3$	1
h_0	$10^3\ pg/cm^3$	1
e_0	$2.5\times10^6\ cell/cm^3$	1
w_0	$4.65\times10^8\ pg/cm^3$	1

doi:10.1371/journal.pone.0110126.t012

arrival of MDSCs to the tumor microenvironment is somewhat delayed and therefore the number of $CD8^+$ T cells in the control case is significantly less than in the J558-IL-35 case, while (for simplicity) our model does not include such a time delay.

The subunits of IL-35, EBI3 and IL-12p35, are highly expressed in cancers such as lung cancer, colorectal cancer, and esophageal carcinoma [2,3]. Anti-IL-35 drug blocks the expression of IL-35 and could be an agent in treating these cancers [48]. To determine the effect of anti-IL-35 drug on cancer growth, we proceed to introduce it, as a drug, into our model. If we denote its concentration by $f(r,t)$ then all we need to do is to modify Equation (4) by

$$\frac{\partial I_{35}}{\partial t}=\underbrace{D_{I_{35}}\frac{1}{r^2}\frac{\partial}{\partial r}\left(r^2\frac{\partial I_{35}}{\partial r}\right)}_{\text{diffusion}}+\frac{1}{f(r,t)}\Bigg[\underbrace{\alpha_{35}c}_{\text{production by tumor}}+\underbrace{\beta_{35}R}_{\text{production by }T_{reg}}+\underbrace{\gamma_{35}M}_{\text{production by MDSC}}\Bigg]-\underbrace{\mu_{35}I_{35}}_{\text{decay}}. \tag{14}$$

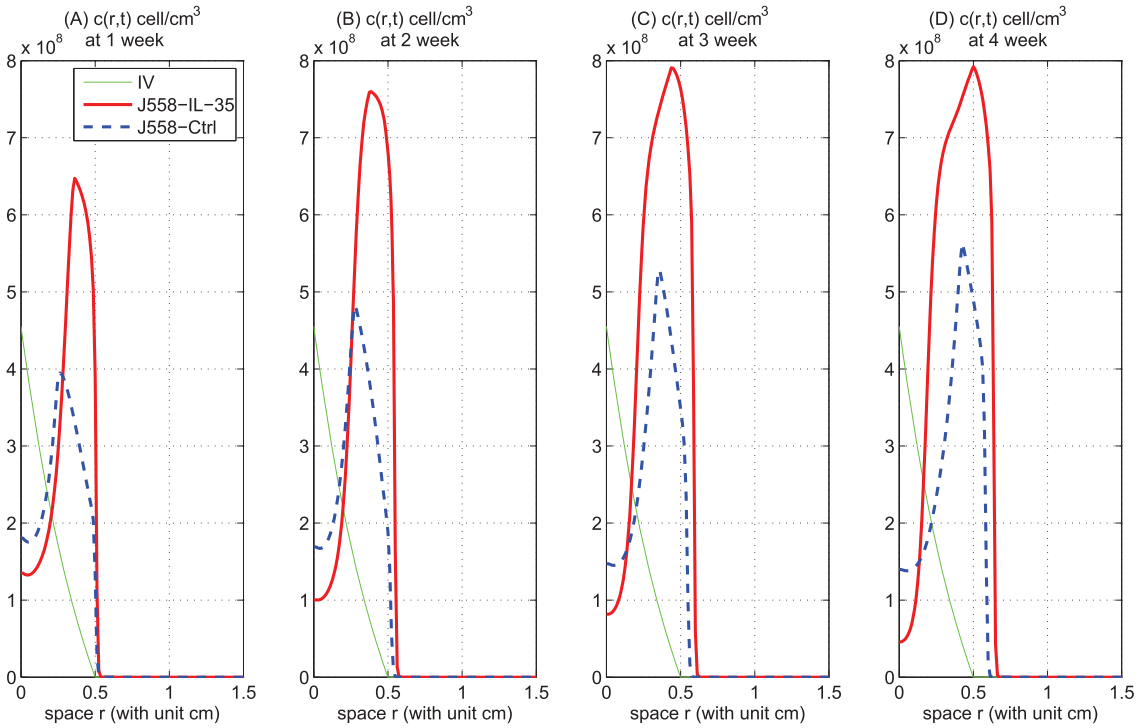

Figure 2. Spatial distributions of tumor cells. (A), (B), (C), and (D) are the spatial distributions of tumor cells $c(r,t)$ in the mice model at the end of the 2nd, 4th, 6th, and 8th weeks, respectively, for cases (i) and (ii). The thin curve is the initial value of tumor cells for the cases (i) and (ii). The solid curve is for J558-IL-35 tumor cells with large I_{35} production (case (ii)) and the dashed curve is for J558-Ctrl tumor cells (case (i)).
doi:10.1371/journal.pone.0110126.g002

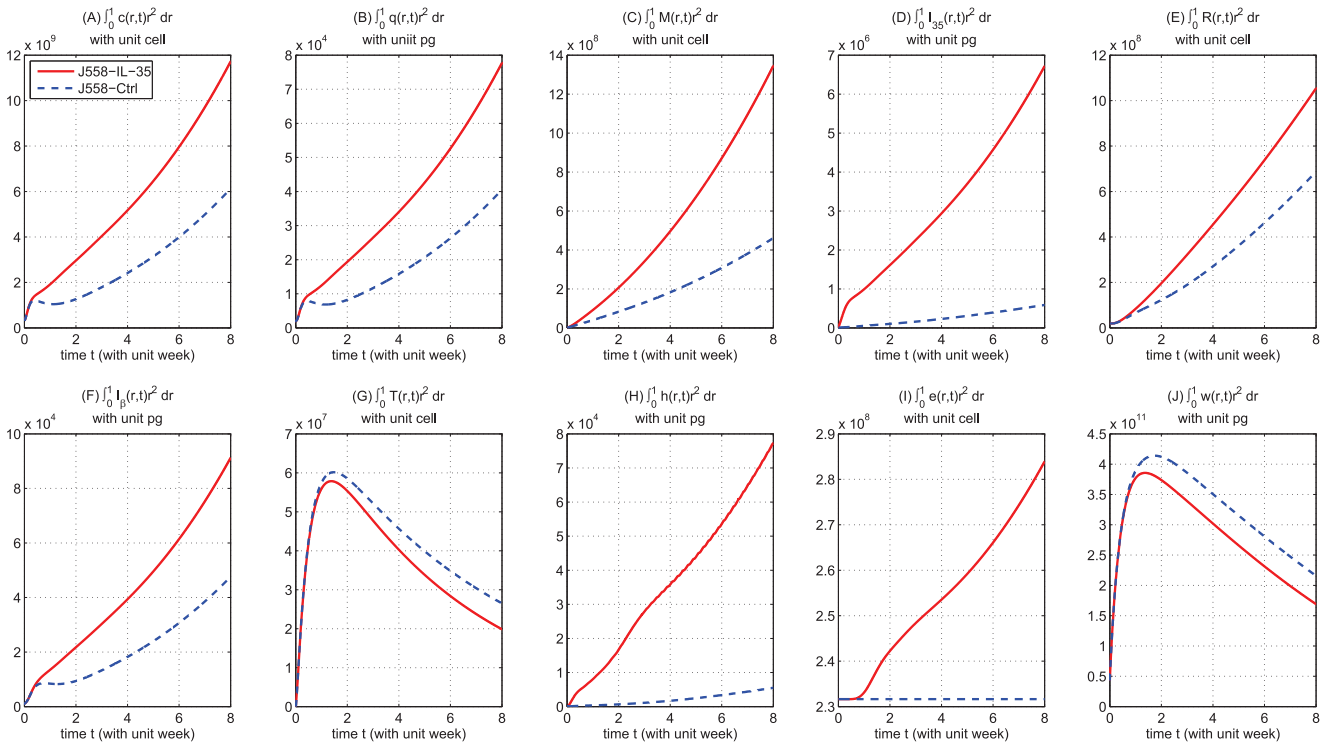

Figure 3. Evolution of cells and cytokines for J558-IL-35 and J558-Ctrl mice models. Panels (A) to (J) show the profiles of the total numbers of tumor cells, M-CSF, MDSCs, I_{35}, T_{reg}s, TGF-β, $CD8^+$ T cells, VEGF, endothelial cells, and oxygen, for cases (i) and (ii). The solid curve is for J558-IL-35 tumor cells with large I_{35} production (case (ii)) and the dashed curve is for J558-Ctrl tumor cells (case (i)).
doi:10.1371/journal.pone.0110126.g003

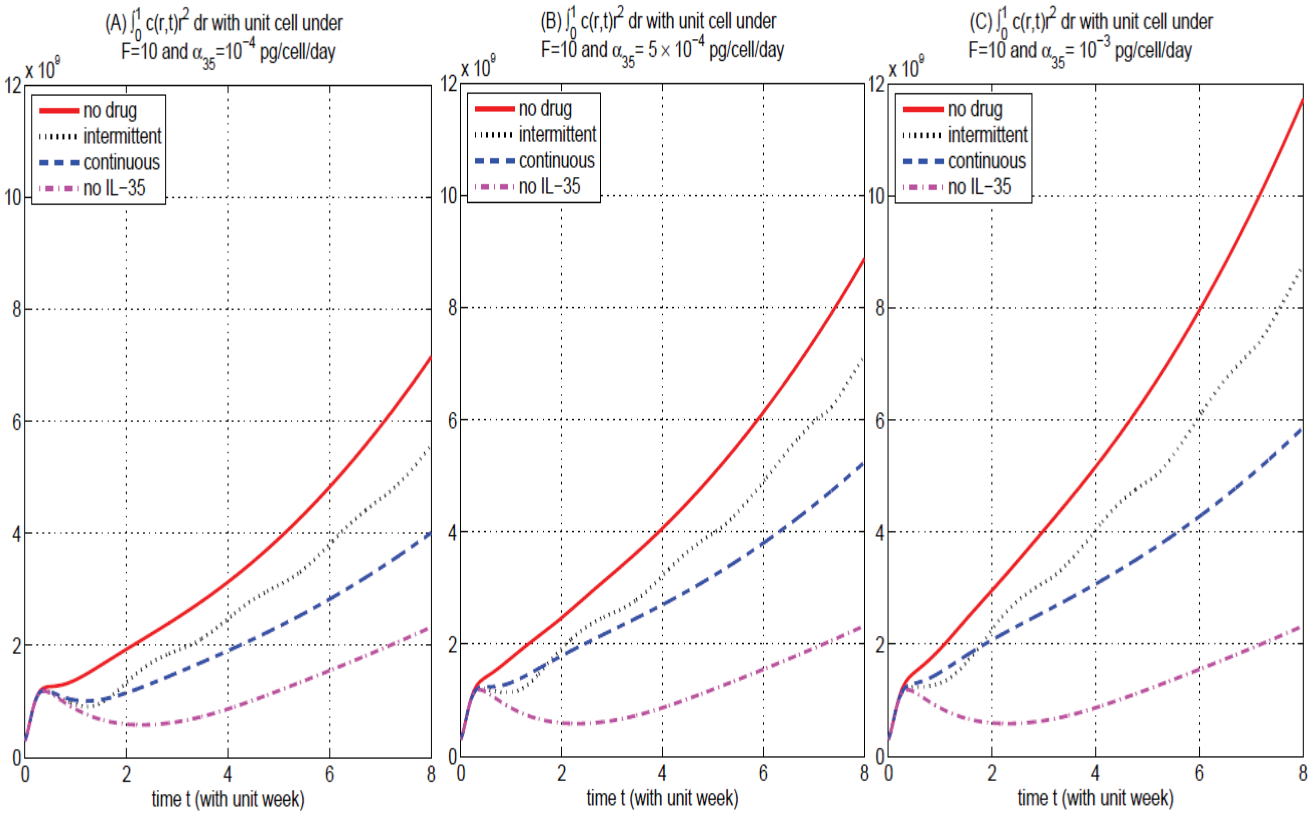

Figure 4. Comparison of continuous versus intermittent treatment in different production rate α_{35} with drug strength $F=10$. (A), (B), and (C) are the profiles of total numbers of $c(r,t)$, under $\alpha_{35}=10^{-4}\ pg/cell/day$, $\alpha_{35}=5\times10^{-4}\ pg/cell/day$, and $\alpha_{35}=10^{-3}\ pg/cell/day$, respectively. The solid curve is for case (i) that no dosing of anti-IL-35 in tumor cells. The dashed and dotted curves are for tumor cells with continuous (case (ii)) and intermittent (case (iii)) drug injections, respectively. The dashed-dot curve $(-.-)$ is the case that there is no IL-35 in the tumor microenvironment, i.e., $\alpha_{35}=\beta_{35}=\gamma_{35}=0$ and $I_{35}(r,0)\equiv0$, for $0\le r\le L$.
doi:10.1371/journal.pone.0110126.g004

We make the pharmacokinetic assumption that $f(r,t)$ decreases in r from the outer boundary of the tumor ($r=1.5\ cm$) towards the center of the tumor ($r=0$), and take

$$f(r,t)=F\times\frac{r^2+a}{L^2+a},\tag{15}$$

where $a=L^2(=2.25\ cm^2)$ and $F=10$. We shall compare several dosing schedules:

(i) no dosing of anti-IL-35, i.e., $f(r,t)=1$, for all t and $0\le r\le L$;

(ii) continuous dosing with anti-IL-35 at fixed level F for 2 months,

$$f(r,t)=F\times\frac{r^2+a}{L^2+a},\ \text{for } 0\le r\le L \text{ and } 0\le t\le 2 \text{ months};\tag{16}$$

(iii) intermittent dosing for 2 months, at double level $2F$, one week at a time with one week spacing between dosing,

$$f(r,t)=\begin{cases}2F\times\dfrac{r^2+a}{L^2+a},\ \text{for } 0\le r\le L \text{ and } t_{2i}\le t<t_{2i+1},\\ 0,\ \text{for } 0\le r\le L \text{ and } t_{2i+1}\le t<t_{2(i+1)},\end{cases}\tag{17}$$

for $i=0, 1, 2, 3$, where $t_0=0$ and the length of each interval $[t_j,t_{j+1}]$ is one week.

We use matlab with $dr=1/80\ cm$ and $dt=7/24000\ day$ in dimensional variables. Figure 4 shows that the temporal growth of the total numbers of tumor cells, as functions of time, under

(A) $\alpha_{35}=10^{-4}\ pg/cell/day$; (B) $\alpha_{35}=5\times10^{-4}\ pg/cell/day$; and (C) $\alpha_{35}=10^{-3}\ pg/cell/day$.

Figure 4 indicates that the continuous treatment has better efficacy in reducing tumor load than intermittent treatment when $\alpha_{35}\in[10^{-4}\ pg/cell/day,\ 10^{-3}\ pg/cell/day]$. Figure 4 also shows that the reduction rate by anti-IL-35 is larger when tumor cells secrete higher amount of IL-35 as in Lung cancer and colorectal cancer [2,3] than lower amount of IL-35 as in plasmacytoma [1]. Accordingly, as α_{35} increases, the reduction in total tumor population becomes increasingly significant.

Sensitivity analysis

In this section we perform sensitivity analysis on the parameters (in dimensional form) including those that were only roughly estimated and those that play important role in the model. We list these parameters with their ranges, baselines, and units in Table 13. We use the method described in Marino et al. [49], using the Latin hypercube sampling to generated 500 samples with $dr=1/40\ cm$ and $dt=7/12000\ day$.

Table 13. Parameters chosen for sensitivity analysis.

Parameter	Range	Baseline	Unit
α_M	$[3.75\times10^{-1},1.5]$	7.5×10^{-1}	$/day$
δ_M	$[6.25\times10^{5}, 2.5\times10^{6}]$	1.25×10^{6}	$cell/cm^3/day$
δ_β	$[1.6635\times10^{6}, 6.654\times10^{6}]$	3.327×10^{6}	$cell/cm^3/day$
α_{35}	$[10^{-5}, 10^{-3}]$	5×10^{-4}	$pg/cell/day$
β_{35}	$[8.35\times10^{-4}, 3.34\times10^{-3}]$	1.67×10^{-3}	$pg/cell/day$
γ_{35}	$[5\times10^{-5}, 2\times10^{-4}]$	10^{-4}	$pg/cell/day$
v_c	$[2.75\times10^{-6}, 1.1\times10^{-5}]$	5.5×10^{-6}	$pg/cell/day$
v_R	$[4.5\times10^{-7}, 1.8\times10^{-6}]$	9×10^{-7}	$pg/cell/day$
η_c	$[1.5787\times10^{-6}, 6.3148\times10^{-6}]$	3.1574×10^{-6}	$cm^3/cell/day$
σ_0	$[2.75863\times10^{4}, 1.10345\times10^{5}]$	5.51725×10^{4}	$cell/cm^3/day$
σ_1	$[2.32759\times10^{2}, 9.31036\times10^{2}]$	4.65518×10^{2}	$/day$
σ_R	$[5\times10^{6}, 2\times10^{7}]$	10^{7}	$cell/cm^3$
σ_β	$[1.2\times10^{3}, 4.8\times10^{3}]$	2.4×10^{3}	pg/cm^3
σ_h	$[1.85\times10^{5}, 7.4\times10^{5}]$	3.7×10^{5}	pg/cm^3
c_M	$[5\times10^{4}, 2\times10^{5}]$	10^{5}	pg/cm^3
s_β	$[1.45\times10^{3}, 5.8\times10^{3}]$	2.9×10^{3}	pg/cm^3
s_M	$[2.5\times10^{6}, 10^{7}]$	5×10^{6}	$cell/cm^3$
a_1	[1,4]	2	$pg/cell$
a_2	$[5\times10^{-3}, 2\times10^{-2}]$	10^{-2}	$pg/cell$
a_3	$[5\times10^{-3}, 2\times10^{-2}]$	10^{-2}	$pg/cell$
k_1	$[1.85\times10^{2}, 7.4\times10^{2}]$	3.7×10^{2}	pg/cm^3
k_2	[5,20]	10	pg/cm^3
λ_1	[1.25,5]	2.5	$/day$
λ_5	$[1.43\times10^{-4}, 5.72\times10^{-4}]$	2.86×10^{-4}	$pg/cell/day$
λ_6	$[7.9\times10^{-4}, 3.16\times10^{-3}]$	1.58×10^{-3}	$pg/cell/day$
λ_{10}	$[2.42352\times10^{-3}, 9.69408\times10^{-3}]$	4.84704×10^{-3}	$cm^3/cell/day$
λ_{12}	$[8.75\times10^{-1}, 3.5]$	1.75	$/day$
e_1	$[3.75\times10^{6}, 1.5\times10^{7}]$	7.5×10^{6}	$cell/cm^3$
h_1	$[7.4\times10^{2}, 2.96\times10^{3}]$	1.48×10^{3}	pg/cm^3

doi:10.1371/journal.pone.0110126.t013

Since we focus on how anti-IL-35 drug inhibits tumor growth, we calculate the partial rank correlation coefficients (PRCC) and p-value, corresponding to the ratio $C := \int_0^1 c^-(r,t)r^2dr / \int_0^1 c(r,t)r^2dr$ for $t=2$ months, where $c^-(r,t)$ accounts for continuous treatment and $c(r,t)$ accounts for of no drug; C is a measure of the (relative) efficacy of the drug. In this analysis, all the parameters are chosen in the range from half to twofold of their baseline, except α_{35} which is chosen from $10^{-5}\ pg/cell/day$ to $10^{-3}\ pg/cell/day$. Table 14 lists the PRCC and their p-values. Figure 5 plots the PRCC of the parameters with p-values smaller than 0.01. A negative PRCC (i.e. negative correlation) with p-value smaller than 0.01 means that increasing this parameter value will decrease the value of C and hence increase the (relative) efficacy of the drug. A positive PRCC with p-value smaller than 0.01 has the opposite meaning, that is, it will decrease the efficacy of the drug.

In Table 14, only η_c, e_1, λ_5, s_M, s_β, α_{35}, and β_{35} have negative PRCC with p-value smaller than 0.01. The most significant negatively correlated parameter is η_c. Larger λ_5 increases the production of VEGF and larger α_{35} increases the production of I_{35} and both increase tumor load. The negative correlation of these parameters shows that the drug is more effective for tumor with higher rate of production of VEGF and IL-35. On the other hand, the negative correlation of η_c shows that the efficacy of the drug improves when the $CD8^+$ T cells are more affective in killing tumor cells. However, it is not true to conclude that, in general, the drug efficacy increases with larger tumor load, since larger η_c and s_β shrink the tumor load but yield better drug efficacy. Similar results hold for the parameters with positive PRCC. For example, larger λ_1 and σ_0 lead to higher tumor cell population while the tumor efficacy is decreased.

Discussion

IL-35 is the most anti-inflammatory cytokine within the IL-12 cytokine family. In this paper we addressed the questions to what extend IL-35 is involved in tumor microenvironment and how effective is anti-IL-35 drug in reducing tumor growth. It is well known that T_{reg}s are presented in the tumor microenvironment

Table 14. The PRCC and p-value of parameters for sensitivity analysis.

Parameter	PRCC	p-value
α_M	−0.00039409	>0.01
δ_M	−0.040652	>0.01
δ_β	−0.045366	>0.01
α_{35}	−0.15449	<0.01
β_{35}	−0.12796	<0.01
γ_{35}	0.055333	>0.01
v_c	0.17422	<0.01
v_R	0.021612	>0.01
η_c	−0.7056	<0.01
σ_0	0.22963	<0.01
σ_1	0.074071	>0.01
σ_R	−0.03105	>0.01
σ_β	0.022536	>0.01
σ_h	0.14064	<0.01
c_M	0.012563	>0.01
s_β	−0.20223	<0.01
s_M	−0.25416	<0.01
a_1	0.33607	<0.01
a_2	−0.0067372	>0.01
a_3	0.014791	>0.01
k_1	0.06582	>0.01
k_2	−0.070145	>0.01
λ_1	0.75819	<0.01
λ_5	−0.26421	<0.01
λ_6	−0.00097113	>0.01
λ_{10}	0.040952	>0.01
λ_{12}	−0.093337	>0.01
e_1	−0.30227	<0.01
h_1	0.28538	<0.01

doi:10.1371/journal.pone.0110126.t014

and that they secrete IL-35 to promote tumor growth. Recent mouse experiments of Wang et al. [1] determined the extend to which IL-35 enhanced the MDSC population and the VEGF concentration, and at the same time decreased the $CD8^+$ T cell population. Based on these experiments, we developed a mathematical model which includes in addition to tumor cells, MDSCs, $CD8^+$ T cells, IL-35, and VEGF, also T_{reg}s, endothelial cells, oxygen concentration, TGF-β, and M-CSF that is produced by cancer cells. The model is described by a system of partial differential equations. The simulations of the model are in qualitative agreement with the experimental results of Wang et al. [1].

We next extended the model to include anti-IL-35 as an anti-cancer drug. We compared the efficacy of the drug under two schedules: continuous versus intermittent injections of the same total amount of the drug. We found that continuous injection has better efficacy while the treatment is ongoing. Since it is well known that some cancers including lung and colorectal cancers most likely secrete large amounts of IL-35, we also investigated the efficacy of the drug for such cancers. We found that the percentage of tumor reduction under anti-IL-35 drug improves when the production of IL-35 by cancer is increased.

There are currently only few experimental results by which our model can be tested. In recent experiments by Nicholl et al. [50] it was demonstrated that IL-35 promotes pancreatic cancer cells proliferation while anti-IL-35 reduces this promotion. More specifically, in Figure three of Nicholl et al. [50] it is shown that IL-35 ($50\ ng/ml$) increases, on the average, by 100% the proliferation of colonies of several pancreatic cancer cell lines, while in the presence of anti-IL-35 ($200\ ng/ml$) this increase is reduced to 50%. These *in vitro* results are in qualitative agreement with our results in Figure three (at week 8). Another example is taken from colorectal cancer in patients. As reported in Zeng et al. [2]. $Foxp3^+T_{reg}$ increases linearly with IL-35, and this is in qualitative agreement with Figures 3D and 3E of our simulations. As more experimental and clinical data become available, we should be able to test our model in more quantitative way, so that the model can further be refined.

In this paper we focused on the role of IL-35, although T_{reg} secrete besides IL-35 also other cytokines that promote tumor, such as IL-10 and IL-9 [7,51–54]; these were not included directly in the present model, since we wanted to base the model on the recent experimental data by Wang et al. [1]. When data for other cytokines become available to the same precision as, for instance, in [1], our model could then be extended to include these cytokines, and to obtain a more comprehensive evaluation of anti-IL-35 efficacy in combination with other drugs.

Methods

Estimate D_c, η_c and λ_1 in Equation (1)

We assume that the killing efficiency of tumor cells by $CD8^+$ T cells is suppressed by IL-35 and that the proliferation rate of tumor cells is enhanced by IL-35. Accordingly in Equation (1), we choose smaller killing rate η_c [55,56] and larger proliferation rate λ_1 of tumor cells than in [22,55]. For simplicity, we take all cells to have the same diffusion coefficient, $D_c = D_M = D_R = D_T = D_e$, with $D_e = 4.32 \times 10^{-6}\ cm^2/day$ by [22,25,57].

Estimate c_M in Equation (3)

From Figures two B and three B in [1], we deduce that I_{35} grows slowly in time, and

$$I_{35}(0) \approx 1.8 \times 10^5\ pg/cm^3 \text{ and } I_{35}(15) \approx 5.6 \times 10^5\ pg/cm^3. \quad (18)$$

We take $c_M = 10^6\ pg/cm^3$ so that on the average $\frac{I_{35}}{I_{35}+c_M} \approx \frac{1}{5}$, for $0 < t < 15$ days.

Estimate σ_0, σ_1, and α_M in Equation (3)

In order to estimate σ_1, we use simplified forms of Equation (3):

$$\frac{dM}{dt} = \sigma_0 + \alpha_M \times \frac{qM_0}{\sigma_M + q} - \mu_M M, \quad (19)$$

$$\frac{d\tilde{M}}{dt} = \sigma_0 + \sigma_1 M_0 \times \frac{I_{35}}{I_{35}+c_M} + \alpha_M \times \frac{qM_0}{\sigma_M + q} - \mu_M \tilde{M}, \quad (20)$$

for J558-Ctrl tumor cells and J558-IL-35 tumor cells, respectively. Taking the difference and recalling that on the average $\frac{I_{35}}{I_{35}+c_M} \approx \frac{1}{5}$ for $0 < t < 15$, we get, with $\mu_M = 0.03/day$ [58,59],

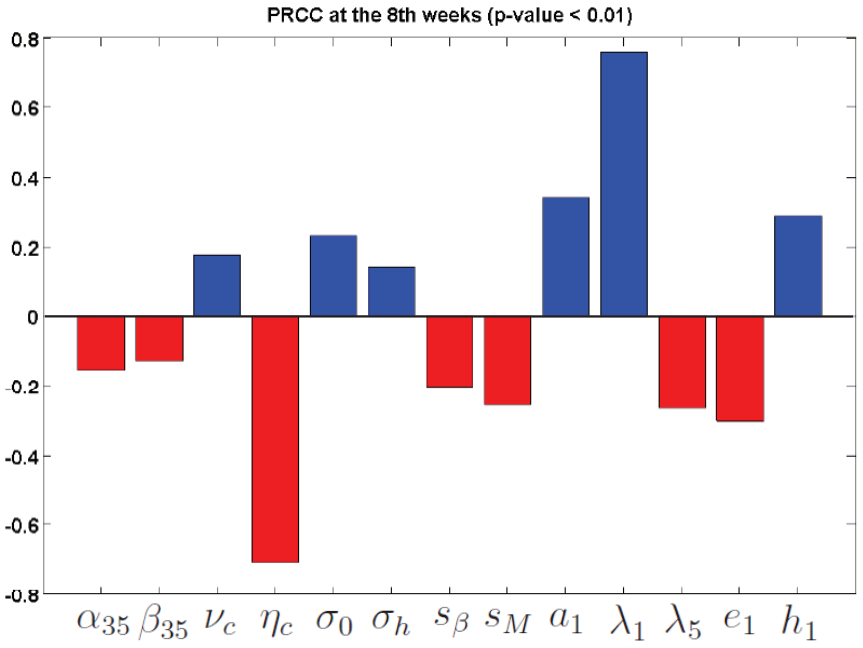

Figure 5. Sensitivity analysis. PRCC values at the second months for the parameters in Table 14 with p-value smaller than 0.01.
doi:10.1371/journal.pone.0110126.g005

$$\tilde{M}(15)-M(15)=(\tilde{M}(0)-M(0))e^{-0.45}+\frac{\sigma_1 M_0}{5\mu_M}(1-e^{-0.45})$$

and the first term of the right-hand side may be neglected since initially the density of MDSC is small [1]. From Figure five A in [1], we deduce that

$$\begin{aligned}&\tilde{M}(15)\approx 18\times 10^6\ cell/cm^3/day \text{ and}\\ &M(15)\approx 9\times 10^6\ cell/cm^3/day.\end{aligned} \tag{21}$$

Since $M_0=8000\ cell/cm^3$ [56,58], we get

$$\begin{aligned}\sigma_1&=\frac{5}{8000\ cell/cm^3}\times\frac{0.03/day\times 9\times 10^6\ cell/cm^3}{1-e^{-0.45}}\\ &\approx 465.518/day.\end{aligned}$$

We assume that, due to the secretion of IL-35, the production of MDSC in the present model is larger than the production assumed in [56], so we have taken σ_0 and α_M to be larger than in [56].

Estimate $D_{I_{35}}$ and μ_{35} in Equation (4)

Since IL-35 belongs to the IL-12 family, we assume that its diffusion coefficient and its degradation rate are the same as for IL-12 [60–63]:

$$D_{I_{35}}=1.25\times 10^{-3}\ cm^2/day,$$

$$\mu_{35}=2/day.$$

Estimate α_{35}, β_{35}, γ_{35} in Equation (4)

In order to find α_{35} for the J558-IL-35 mouse model, we use the simplified version of Equation (4) where only cancer cells produce I_{35}, i.e., $R=0$ and $M=0$:

$$\frac{dI_{35}(t)}{dt}=\alpha_{35}c-\mu_{35}I_{35}(t). \tag{22}$$

If c is taken to be a constant, then

$$I_{35}(t)=e^{-\mu_{35}t}I_{35}(0)+\frac{\alpha_{35}c}{\mu_{35}}(1-e^{-\mu_{35}t}). \tag{23}$$

In the *in vivo* experiments of Wang et al. [1] the initial number of cancer cells that were injected was 5×10^6 and we assume that they occupy a volume of 50 mm^3, so that

$$c(0)=10^8\ cell/cm^3. \tag{24}$$

There is no data in [1] on the density of the tumor cells in day 15, but the tumor cells were observed to grow rapidly in the first 15 days. We assume that the average of the density of tumor cells in the first 15 days is very close to the maximal capacity $10^9\ cell/cm^3$ and take, in (23), $c=10^9\ cell/cm^3$ for J558-IL-35 tumor cells. Recalling Equation (18), we get, with $\mu_{35}=2/day$ (Table 4),

$$5.6\times 10^5\ pg/cm^3\approx e^{-15\ day\times 2/day}\times 1.8\times 10^5\ pg/cm^3$$

$$+\frac{\alpha_{35}}{2/day}\times 10^9\ cell/cm^3\times(1-e^{-15\ day\times 2/day}),$$

so that $\alpha_{35}\approx 10^{-3}\ pg/cell/day$ for J558-IL-35 mouse model.

In contrast to the case of J558-IL-35 mouse model, in J558-Ctrl mouse I_{35} is mainly secreted by T_{reg}s [11,13,14,27], little by MDSCs, and very little by tumor cells. Hence, in the J558-Ctrl case, we take the production rate of I_{35} by tumor cells to be $\alpha_{35}=10^{-7}\ pg/cell/day$.

The production rate of I_{35} by T_{reg} is estimated to be $\beta_{35}=1.67\times 10^{-3}\ pg/cell/day$ [34] and we take the production rate of I_{35} by MDSCs to be small enough, i.e., $\gamma_{35}=10^{-4}\ pg/cell/day$, so that the production of I_{35} in the J558-IL-35 case satisfies:

$$\alpha_{35}c\gg\beta_{35}R\gg\gamma_{35}M,$$

and production of I_{35} in J558-Ctrl case satisfies:

$$\beta_{35}R\gg\gamma_{35}M\gg\alpha_{35}c.$$

Estimate δ_M, δ_β, σ_R, σ_β in Equation (5)

In [38], the cytokine signalling by TGF-β on T_{reg} is modeled by

$$\tilde{\delta}_\beta\frac{I_\beta}{I_\beta+\tilde{\sigma}_\beta},\tag{25}$$

where $\tilde{\delta}_\beta=33.27/day$ which has dimension per day and $\tilde{\sigma}_\beta=1$ which is nondimension. In our Equation (5), the dimension of δ_β is $cell/cm^3/day$ and the dimension of σ_β is pg/cm^3. Correspondingly, we take

$$\delta_\beta=\tilde{\delta}_\beta\times R_0=33.27/day\times 10^5\ cell/cm^3=$$
$$3.327\times 10^6\ cell/cm^3/day,$$

$$\sigma_\beta=\tilde{\sigma}_\beta\times I_\beta^0=1\times 2.4\times 10^3\ pg/cm^3=2.4\times 10^3\ pg/cm^3,$$

where $I_\beta^0\approx 2.4\times 10^3\ pg/cm^3$ [64].

MDSC also activates T_{reg} population. We assume that the activation of T_{reg} by MDSC is weaker than the activation of T_{reg} by TGF-β, and hence take it to be

$$\delta_M=\frac{3}{8}\delta_\beta\approx 1.25\times 10^6\ cell/cm^3/day.$$

We also take $\sigma_R=10^7\ cell/cm^3$.

Estimate v_c and v_R in Equation (6)

We assume as before that the initial tumor occupies a volume of $50\ mm^3$ and, accordingly, also T_{reg} occupies the same volume. In [34], the production of I_β by tumor cells and T_{reg}s are $1.1\times 10^{-4}\frac{pg}{day\cdot cell}\times\frac{1}{cm^3}$ and $1.8\times 10^{-5}\frac{pg}{day\cdot cell}\times\frac{1}{cm^3}$, respectively. Hence,

$$v_R=1.8\times 10^{-5}\frac{pg}{day\cdot cell}\times\frac{1}{cm^3}\times 50\ mm^3=9\times 10^{-7}\ pg/cell/day,$$

$$v_c=1.1\times 10^{-4}\frac{pg}{day\cdot cell}\times\frac{1}{cm^3}\times 50\ mm^3=5.5\times 10^{-6}\ pg/cell/day.$$

Estimate s_M, β_1, β_2, a_1, a_2, a_3, c_5 in Equation (7)

Since IL-35 enhances the population of MDSC, the concentration of IL-10, which we represent by a_1M, is larger than the one in [56]. Hence, we chose s_M to be larger than the corresponding value of s_M in [56]. Moreover, since IL-35 promotes tumor growth, we expect a stronger immune response by T cells than in [56] and hence we take β_1 and β_2 larger than the corresponding value in [56]. The parameter c_5 is taken from [56]. Since the chemotaxis and activation of $CD8^+$ T cells are indirect, we take a_2 and a_3 to be smaller than a_1: $a_1=2\ pg/cell$ and $a_2=a_3=0.01\ pg/cell$.

Estimate k_1, k_2, σ_h, λ_5, w_* in Equation (8)

We take σ_h to be the average of the concentration of IL-35 at times 0 and 15 days, so that $\sigma_h=3.7\times 10^5\ pg/cm^3$ by Equation (18). We assume that the productions of VEGF by tumor cells and MDSCs are small when there are no IL-35 and M-CSF, respectively, so we set $k_1=3.7\times 10^2\ pg/cm^3$ and $k_2=10\ pg/cm^3$. Since in [1] I_{35} increases the concentration of VEGF significantly, we take λ_5 to be larger than the value in [56]. We also slightly modify the parameter value w_* and function ϕ used in [56].

Estimate D_e, k_h, λ_{12}, e_1, h_0, and h_1 in Equation (9)

We take values similar to those in [22,55].

Estimate λ_8, λ_9, and λ_{10} in Equation (10)

We assume that $CD8^+$ T cells, MDSCs, and T_{reg}s have the same consumption rates of oxygen, so we take $\lambda_8=\lambda_9=\lambda_{10}=1.61568\times 10^{-8}\ cm^3/cell/day$ [55,56,65].

Author Contributions

Conceived and designed the experiments: KL XB AF. Performed the experiments: KL XB AF. Analyzed the data: KL XB AF. Contributed reagents/materials/analysis tools: KL XB AF. Wrote the paper: KL XB AF.

References

1. Wang Z, Liu JQ, Liu Z, Shen R, Zhang G, et al. (2013) Tumor-derived il-35 promotes tumor growth by enhancing myeloid cell accumulation and angiogenesis. J Immuno 190: 2415–2423.
2. Zeng JC, Zhang Z, Li TY, Liang YF,Wang HM, et al. (2013) Assessing the role of il-35 in colorectal cancer progression and prognosis. Int J Clin Exp Pathol 6: 1806–1816.
3. Long J, Zhang X, Wena M, Kong Q, Lv Z, et al. (2013) Il-35 over-expression increases apoptosis sensitivity and suppresses cell growth in human cancer cells. Biochemical and Biophysical Research Communications 430: 364–369.
4. Liyanage UK, Moore TT, Joo HG, Tanaka Y, Herrmann V, et al. (2002) Prevalence of regulatory t cells is increased in peripheral blood and tumor microenvironment of patients with pancreas or breast adenocarcinoma. J Immunol 169: 2756–2761.
5. Wolf D, Wolf AM, Rumpold H, Fiegl H, Zeimet AG, et al. (2005) The expression of the regulatory t cell-specific forkhead box transcription factor foxp3 is associated with poor prognosis in ovarian cancer. Clin Cancer Res 11: 8326–8331.

6. Strauss L, Bergmann C, Szczepanski M, Gooding W, Johnson JT, et al. (2007) A unique subset of $cd4^+cd25^{high}foxp3^+$ t cells secreting interleukin-10 and transforming growth factor-β1 mediates suppression in the tumor microenvironment. Clinical Cancer Research 13: 4345–4354.
7. Eller K, Wolf D, Huber JM, Metz M, Mayer G, et al. (2011) Il-9 production by regulatory t cells recruits mast cells that are essential for regulatory t cell-onduced immune suppression. J Immunology 186: 83–91.
8. Collison LW, Workman CJ, Kuo TT, Boyd K, Wang Y, et al. (2007) The inhibitory cytokine il-35 contributes to regulatory t-cell function. Nature 450: 566–569.
9. Collison LW, Vignali DAA (2008) Interleukin-35: odd one out or part of the family? Immunol Rev 226: 248–262.
10. Vignali DAA, Collison LW, Workman CJ (2008) How regulatory t cells work. Nat Rev Immunol 8: 523–532.
11. Xu M, Mizoguchi I, Morishima N, Chiba Y, Mizuguchi J, et al. (2010) Regulation of antitumor immune responses by the il-12 family cytokines, il-12, il-23, and il-27. Clinical and Developmental immunology 14: 832454.
12. Chaturvedi V, Collison LW, Guy CS, Workman CJ, Vignali DAA (2011) Human regulatory t cells require interleukin-35 to mediate suppression and infectious tolerance. J Immunol 186: 6661–6666.
13. Collison LW, Delgoffe GM, Guy CS, Vignali KM, Chaturvedi V, et al. (2012) The composition and signaling of the il-35 receptor are unconventional. Nature immunology 13: 290–299.
14. Vignali DAA, Kuchroo VK (2012) Il-12 family cytokines: immunological playmakers. Nature immunology 13: 722–728.
15. Collison LW, Chaturvedi V, Henderson AL, Giacomin PR, Guy C, et al. (2010) Il-35-mediated induction of a potent regulatory t cell population. Nat Immunol 11: 1093–1101.
16. Nishino R, Takano A, Oshita H, Ishikawa N, Akiyama H, et al. (2011) Identification of epstein-barr virus-induced gene 3 as a novel serum and tissue biomarker and a therapeutic target for lung cancer. Clin Cancer Res 17: 6272–6286.
17. Larousserie F, Bardel E, Pflanz S, Arnulf B, Lome-Maldonado C, et al. (2005) Analysis of interleukin-27 (ebi3/p28) expression in epstein-barr virus- and human t-cell leukemia virus type 1-associated lymphomas: heterogeneous expression of ebi3 subunit by tumoral cells. Am J Pathol 166: 1217–1228.
18. Niedobitek G, Päolt D, Teichmann M, Devergne O (2002) Frequent expression of the epstein-barr virus (ebv)-induced gene, ebi3, an il-12 p40-related cytokine, in hodgkin and reed-sternberg cells. J Pathol 198: 310–316.
19. Gabrilovich DI, Rosenberg SO, Bronte V (2012) Coordinated regulation of myeloid cells by tumors. Nat Rev Immunol 12: 253–268.
20. Yang WC, Ma G, Chen SH, Pan PY (2013) Polarization and reprogramming of myeloid-derived suppressor cells. J Mol Cell Biol 5: 207–209.
21. Kendall M (1998) Dying to live: How our bodies fight disease. Cambridge University.
22. Szomolay B, Eubank TD, Roberts RD, Marsh CB, Friedman A (2012) Modeling the inhibition of breast cancer growth by gm-csf. J Theoret Biol 303: 141–151.
23. Lewis JS, Lee JA, Underwood JCE, Harris AL, Lewis CE (1999) Macrophage responses to hypoxia: relevance to disease mechanisms. J Leuk Biol 66: 889–900.
24. Mantovani A, Sica A, Sozzani S, Allavena P, Vecchi A, et al. (2004) The chemokine system in diverse forms of macrophage activation and polarization. Trends Immunol 25: 677–686.
25. Owen MR, Byrne HM, Lewis CE (2004) Mathematical modeling of the use of macrophages as vehicles for drug delivery to hypoxic tumor sites. J Theore Biol 226: 377–391.
26. Sica A, Schioppa T, Mantovani A, Allavena P (2006) Tumour-associated macrophages are a distinct m2 polarised population promoting tumour progression: Potential targets of anti-cancer therapy. European J of Cancer 42: 717–727.
27. Morishima N, Mizoguchi I, Okumura M, Chiba Y, Xu M, et al. (2010) A pivotal role for interleukin-27 in cd8+ t cell functions and generation of cytotoxic t lymphocytes. J Biomedicine and Biotechnology: doi:10.1155/2010/605483.
28. Baek HJ, Kim SS, da Silva FM, Volpe EA, Evans S, et al. (2006) Inactivation of tgf-beta signaling in lung cancer results in increased cdk4 activity that can be rescued by elf. Biochem Biophys Res Commun 11: 1150–1157.
29. Colombo MP, Piconese S (2007) Regulatory t-cell inhibition versus depletion: the right choice in cancer immunotherapy. Nature Reviews Cancer 7: 880–887.
30. Danforth DNJ, Sgagias MK (1996) Tumor necrosis factor alpha enhances secretion of transforming growth factor beta2 in mcf-7 breast cancer cells. Clin Cancer Res 2: 827–835.
31. Kretzschmar M (2000) Transforming growth factor-beta and brest cancer: transforming growth factor-beta/smad signaling defects and cancer. Breast Cancer Res 2: 107–115.
32. Massagué J (1998) Tgf-beta signal transduction. Annu Rev Biochem 67: 753–791.
33. Muller AJ, Scherle PA (2006) Targeting the mechanisms of tumoral immune tolerance with small-molecule inhibitors. Nat Rev Cancer 6: 613–625.
34. Robertson-Tessi M, El-Kareh A, Goriely A (2011) A mathematical model of tumor-immune interactions. Journal of Theoretical Biology 10: 294–273.
35. Truty MJ, Urrutia R (2007) Basics of tgf-beta and pancreatic cancer. Pancreatology 7: 423–435.
36. Tran DQ (2012) Tgf-β: the sword, the wand, and the shield of $foxp3^+$ regulatory t cells. J Mol Cell Biol 4: 29–37.
37. Kullberg MC, Hay V, Cheever AW, Mamura M, Sher A, et al. (2005) Tgf-beta1 production by $cd4^+cd25^+$ regulatory t cells is not essential for suppression of intestinal inflammation. Eur J Immunol 35: 2886–2895.
38. LoWC, Arsenescu RI, Friedman A (2013) Mathematical model of the roles of t cells in inflammatory bowel disease. Bull Math Biol 75: 1417–1433.
39. Boelte KC, Gordy LE, Joyce S, Thompson MA, Yang L, et al. (2011) Rgs2 mediates pro-angiogenic function of myeloid derived suppressor cells in the tumor microenvironment via upregulation of mcp-1. PLoS ONE 11: e18534.
40. Kross KW, Heimdal JH, Olsnes C, Olofson J, Aarstad HJ (2007) Tumor-associated macrophages secrete il-6 and mcp-1 in head and neck squamous cell carcinoma tissue. Acta Otolaryngol 127: 532–539.
41. Robertson MJ, Ritz J (1996) Interleukin 12: basic biology and potential applications in cancer treatment. Oncologist 1: 88–97.
42. Lai YP, Jeng CJ, Chen SC (2011) The roles of $cd4^+$ t cells in tumor immunity. ISRN Immunology 2011: doi:10.5402/2011/497397.
43. Wagner H, Kronke M, Solbach W, Scheurich P, Rollinghoff M, et al. (1982) Murine t cell subsets and interleukins: relationships between cytotoxic t cells, helper t cells and accessory cells. Clin Haematol 11: 607–630.
44. Tiemessen MM, Kunzmann S, Schmidt-Weber CB, Garssen J, Bruijnzeel-Koomen CA, et al. (2003) Transforming growth factor-beta inhibits human antigen-specific $cd4^+$ t cell proliferation without modulating the cytokine response. Int Immunol 15: 1495–1504.
45. Quatromoni JG, Suzuki E, Okusanya O, Judy BF, Bhojnagarwala P, et al. (2013) The timing of tgf-β inhibition affects the generation of antigen-specific $cd8^+$ t cells. BMC Immunol 17: doi: 10.1186/1471-2172-14-30.
46. Thomas DA, Massagué J (2005) Tgf-β directly targets cytotoxic t cell functions during tumor evasion of immune surveillance. Cancer Cell 8: 369–380.
47. Eubank TD, Roberts RD, Khan M, Curry JM, Nuovo GJ, et al. (2009) Granulocyte macrophage colony-stimulating factor inhibits breats growth and metastasis by invoking an anti-angiogenic program in tumor-educated macrophages. Cancer Res 69: 2133–2140.
48. Lin Y, Huang Y, Lu Z, Luo C, Shi Y, et al. (2012) Decreased plasma il-35 levels are related to the left ventricular ejection fraction in coronary artery diseases. PLoS ONE 7: e52490.
49. Marino S, Hogue IB, Ray CJ, Kirschner DE (2008) A methodology for performing global uncertaintly and sensitivity analysis in systems biology. J Theor Biol 254: 178–196.
50. Nicholl MB, Ledgewood CL, Chen X, Bai Q, Qin C, et al. (2014) Il-35 promotes pancreas cancer growth through enhancement of proliferation and inhibition of apoptosis: Evidence for a role as an autocrine growth factor. Cytokine: in press.
51. Jarnicki A, Lysaght J, Todryk S, Mills K (2006) Suppression of antitumor immunity by il-10 and tgf-β-producing t cells infiltrating the growing tumor: influence of tumor environment on the induction of $cd4^+$ and $cd8^+$ regulatory t cells. J Immunol 177: 896–904.
52. Maynard CL, Harrington LE, Janowski KM, Oliver JR, Zindl CL, et al. (2007) Regulatory t cells expressing interleukin 10 develop from $foxp3^+$ and foxp3*v* precursor cells in the absence of interleukin 10. Nature immunology 8: 931–941.
53. Putheti P, Awasthi A, Popoola J, Gao W, Strom TB (2010) Human $cd4^+$ memory t cells can become $cd4^+il\text{-}9^+$ t cells. PLoS ONE 5: e8706.
54. Schmitt EG, Haribhai D, Williams JB, Aggarwal P, Jia S, et al. (2012) Il-10 produced by induced regulatory t cells (itregs) controls colitis and pathogenic ex-itregs during immunotherapy. J Immunol 189: 5638–5648.
55. Chen D, Roda JM, Marsh CB, Eubank TD, Friedman A (2012) Hypoxia inducible factors mediate the inhibtion of cancer by gm-csf: a mathematical model. Bull Math Biol 17: 2752–2777.
56. Liao KL, Bai XF, Friedman A (2013) The role of cd200-cd200r in tumor immune evasion. J Theor Biol 328: 65–76.
57. Plank MJ, Sleeman BD, Jones PF (2004) A mathematical model of tumor anglogenesis, regulated by vascular endothelial growth factor and the angiopoietins. J Theore Biol 229: 435–454.
58. Day J, Friedman A, Schlesinger LS (2008) Modeling the immune rheostat of macrophages in the lung in response to infection. PNAS 106: 11246–11251.
59. Freeman BJ, Roberts MS, Vogler CA, Nicholes A, Hofling AA, et al. (1999) Behavior and therapeutic efficacy of β-glucuronidase-positive mononuclear phagocytes in murine model of mucopolysaccharidosis type vii. Blood 94: 2142–2150.
60. DiLeo MV, Kellum JA, Federspiel WJ (2009) A simple mathematical model of cytokine capture using a hemoadsorption device. Ann Biomed Eng 37: 222–229.
61. Sánchez-Hernández C, Gutiérrez-Ortega A, Aguilar-León D, Hernández-Pando R, Gómez-Lim M, et al. (2010) In vivo activity of plant-based interleukin-12 in the lung of balb/c mouse. BMC Research Notes 3: doi: 10.1186/1756-0500-3-151.
62. Lee SM, Suen Y, Chang L, Bruner V, Qian J, et al. (1995) Decreased interleukin-12 (il-12) from activated cord versus adult peripheral blood mononuclear cells and upregulation of interferongamma, natural killer, and lyphokine-activated killer activity by il-12 in cord blood mononuclear cells. Blood 88: 945–954.
63. Robertson MJ, Cameron C, Atkins MB, Gordon MS, Lotze MT, et al. (1999) Immunological effects of interleukin 12 administered by bolus intravenous injection to patients with cancer. Clin Cancer Res 5: 9–16.
64. Todorović-Raković N, Ivanović V, Demajo M, Nešković-Konstantinovi Z, Nikolić-Vukosavljević D (2003) Elevated plasma levels of tgf-beta1 in patients with locally advanced breast cancer related to other clinical stages. Archive of Oncology 11: 131–133.

65. Youn BS, Sen A, Behie LA, Girgis-Gabardo A, Hassell JA (2008) Scale-up of breast cancer stem cell aggregate cultures to suspension bioreactors. Biotechnol Prog 22: 801–810.
66. Breward CJW, Byrne HM, Lewis CE (2001) Modeling the interactions between tumor cells and a blood vessel in a microenvironment within a vascular tumor. European J Appl Math 12: 529–556.
67. Qian B, Deng Y, Hong Im J, Muschel RJ, Zou Y, et al. (2009) A distinct macrophage population mediated metastatic breast cancer cell extravasation, establishment and growth. PLoS ONE 4: e6563.
68. Vaupel P, Mayer A, Briest S, Höckel M (2003) Oxygenation gain factor: a novel parameter characterizing the association between hemoglobin level and the oxygenation status of breast cancers. Cancer Res 63: 7634–7637.
69. Casciari JJ, Sotirchos SV, Sutherland RM (1988) Glucose diffusivity in multicellular tumor spheroids. Cancer Res 48: 3905–3909.
70. Owen MR, Sherratt JA (1998) Pattern formation and spatiotemporal irregularity in a model for macrophage tumor interactions. J Theore Biol 189: 63–80.
71. Oren H, Duman N, Abacioglu H, Ozkan H, Irken G (2001) Association between serum macrophage colony-stimulating factor levels and monocyte and thrombocyte counts in healthy, hypoxic, and septic term neonates. Pediatrics 108: 329–332.
72. Utting JC, Flanagan AM, Brandao-Burch A, Orriss IR, Aenett TR (2010) Hypoxia stimulates osteoclast formation from human peripheral blood. Cell Biochem Funct 28: 374–380.
73. Tang S, Liu H, Chen G, Rao Q, Geng Y, et al. (2000) Internalization and half-life of membrane-bound macrophage colony-simulating factor. Chinese Sc Bull 45: 1697–1703.
74. Vukmanovic-Stejic M, Zhang Y, Cook J, Fletcher J, McQuaid A, et al. (2006) Human $cd4^{+}cd25^{hi}$foxp3 regulatory t cells are derived by rapid turnover of memory populations in vivo. J Clin Invest 116: 2423–2433.
75. Yates A, Callard R (2001) Cell death and the maintenance of immunological memory. Discret Contin Dyn S 1: 43–59.
76. Kim Y, Friedman A (2010) Interaction of tumor with its micro-environment: a mathematical model. J Math Biol 72: 1029–1068.
77. Marino S, Kirschner DE (2004) The human immune response to mycobacterium tuberculosis in lung and lymph node. J Theor Biol 227: 463–486.
78. Abe R, Donnelly SC, Peng T, Bucala R, Metz CN (2001) Peripheral blood fibrocytes: differentiation pathway and migration to wound sites. J Immunol 166: 7556–7562.
79. Kim Y, Lawler S, Nowicki MO, Chiocca EA, Friedman A (2009) A mathematical model for pattern formation of glioma cells outside the tumor spheroid core. J Theore Biol 260: 359–371.
80. Kim Y, Wallace J, Li F, Ostrowski M, Friedman A (2010) Transfirmed epithelial cells and fibroblasts/myofibroblasts interaction in breast tumor: a mathematical model and experiments. J Math Biol 61: 401–421.
81. Hengel RL, Jones BM, Kennedy MS, Hubbard MR, McDougal JS (1999) Markers of lymphocyte homing distinguish cd4 t cell subsets that turn over in response to hiv-1 infection in humans. J Immunol 163: 3539–3548.
82. Sachsenberg N, Perelson AS, Yerly S, Schockmel GA, Leduc D, et al. (1998) Turnover of cd4+ and cd8+ t lymphocytes in hiv-1 infection as measured by ki-67 antigen. J Exp Med 187: 1295–1303.
83. Sprent J, Basten A (1973) Circulating t and b lymphocytes of the mouse. ii. lifespan. Cell Immunol 7: 40–59.
84. Wigginton JE, Kirschner D (2001) A model to predict cell-mediated immune regulatory mechanisms during human infection with mycobacterium tuberculosis. J Immunol 166: 1951–1967.
85. Winslow GM, Roberts AD, Blackman MA, Woodland DL (2003) Persistence and turnover of antigen-specific cd4 t cells during chronic tuberculosis infection in the mouse. J Immunol 170: 2046–2052.
86. Gabhann FM, Popel AS (2003) Model of competitive binding of vascular endothelial growth factor and placental growth factor to vegf receptors on endothelial cells. Am J Physiol Heart Circ Physiol 286: H153–H164.
87. Schugart RC, Friedman A, Zhao R, Sen CK (2008) Wound angiogenesis as a function of tissue oxygen tension: a mathematical model. PNAS 105: 2628–2633.
88. Chaplain MAJ, Giles SM, Sleeman BD, Jarvis RJ (1995) Amathematical analysis of a model for tumour angiogenesis. J Math Biol 33: 744–770.
89. Eubank TD, Roberts R, Galloway M, Wang Y, Cohn DE, et al. (2004) Gm-csf induces expression of soluble vegf receptor-1 from human monocytes and inhibits angiogenesis in mice. Immunity 21: 831–842.
90. Chaplain MAJ (1995) The mathematical modeling of tumour angiogenesis and invasion. Acta Biotheoret 43: 387–402.
91. Butterworth AE, Cater DB (1967) Effect of lysolecithin on oxygen uptake of tumor cells polymorphonuclear leucocytes lymphocytes and macrophages in vitro. Br J Cancer 21: 373–389.
92. Chen Y, Cairns R, Papandreou I, Koong A, Denko NC (2009) Oxygen consumption can regulate the growth of tumors, a new perspective on the warburg effect. PLoS ONE 4: e7033.